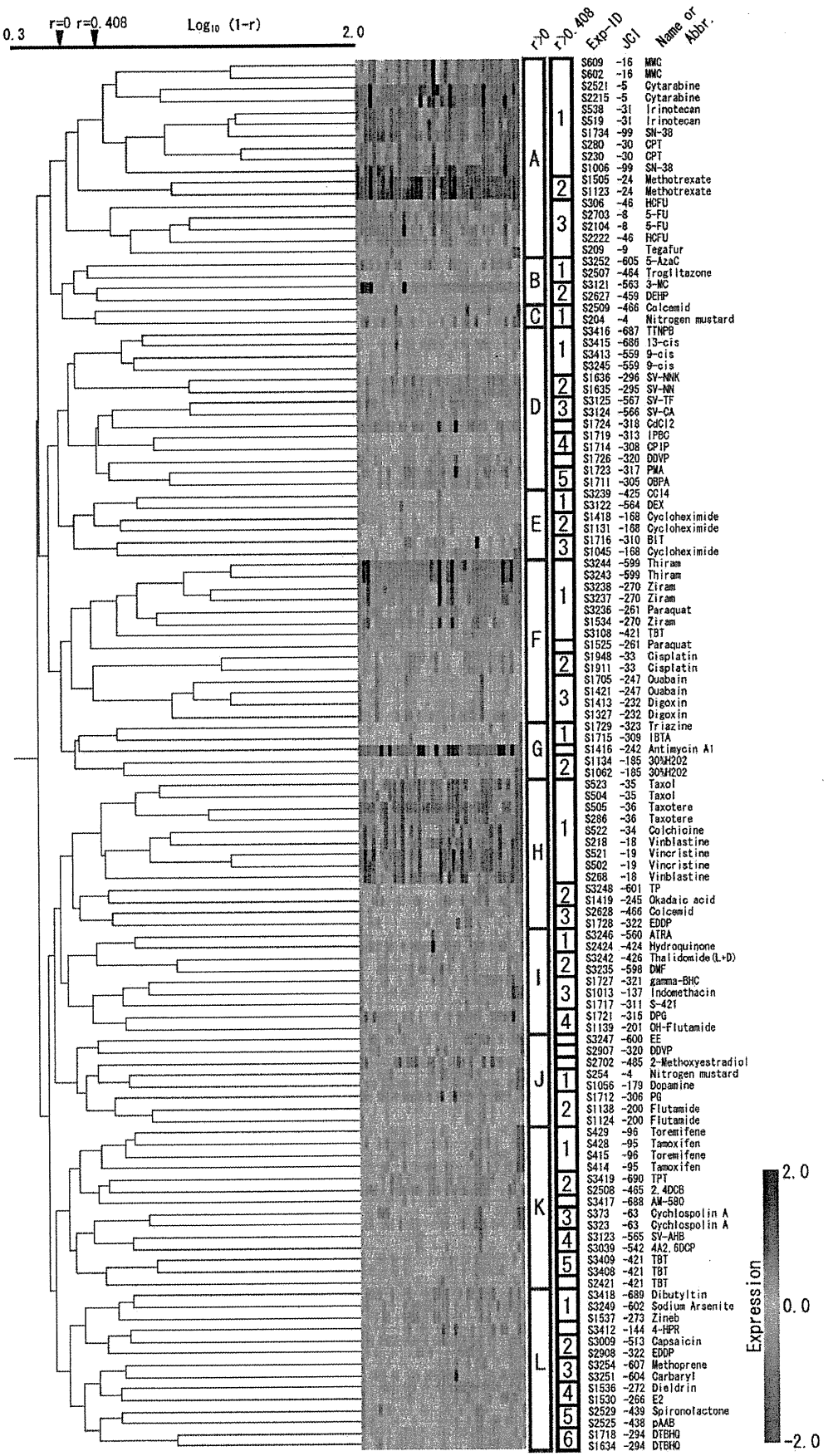

Fig. 3. Hierarchical clustering of 69 test chemicals and 20 anticancer drugs based on their GI50 values. Hierarchical clustering method was an "average linkage method" using the Pearson correlation as distance. We classified the chemicals into two kinds of clusters; their threshold values were $r = 0$ and $r = 0.408$ ($p < 0.01$), respectively. Gradient color indicates relative level (log transformed) of GI50. Red, more sensitive than the mean GI50 (2.0); yellow, mean GI50 (0.0); and green, less sensitive than the mean GI50 (−2.0). On the color scale, red represents the GI50 value that is 100-fold higher than the mean GI50.

NNK and SV-NN, on the other hand, belonged to the cluster D2. These results are in accordance with the similar fingerprints shown in Fig. 2. It is noteworthy that the snake venoms from the *C. atrox* and *T. flavoviridis*, species belonging to the viperidae family of snakes, formed another cluster (cluster D3), which was different from that of the elapidae family of snakes, *N. naja kaouthia* and *N. nigricollis*. 9-*cis* Retinoic acid, 13-*cis* retinoic acid, and 4-[*E*-2-(5,6,7,8-tetrahydro-5,5,8,8-tetra-methyl-2-naphthalenyl)-1-propenyl]benzoic acid, which are RAR agonists (Aström et al., 1990), also formed a separate cluster (cluster D1). Likewise, agricultural chemicals paraquat, ziram, and thiram formed a single cluster (cluster F1).

Discussion

The JFCR39 system coupled to a drug activity database is a good model for investigating the diversity of chemosensitivity in cancer cells. We have previously established panels of human cancer cell lines [JFCR39 (Yamori, 2003) and JFCR45 (Nakatsu et al., 2005)]. We used these panels of cells to demonstrate that they provide powerful means to predict the action mechanisms of drugs, and also used them to identify new target compounds. In this manuscript, we used the JFCR39 system to evaluate various chemicals (such as toxic chemicals, agricultural chemicals, and synthetic intermediates), which are not anticancer drugs, and classified them according to their molecular target or action mechanism. As a result, these chemicals were classified into a number of clusters. Our results also suggested that each cluster consisted of chemicals sharing a common action mechanism.

We determined the growth inhibition of cells in the JFCR39 panel by 130 chemicals and calculated their GI50 values. Some of the chemicals were assessed twice or more to confirm the reproducibility of the assay. We had to exclude 61 chemicals from further analysis because they did not inhibit the cells in the JFCR39 panel significantly. The rest of the chemicals (69 of 130, ~60%) met our selection criteria and were evaluated by cluster analysis.

First, we found that the chemicals tested in duplicate formed tight clusters, showing high reproducibility. Next, we investigated the difference between these 69 test chemicals and the anticancer drugs. Sixty-nine chemicals, which are not anticancer drugs, formed several clusters, which were different from the anticancer drug clusters. These results suggest that the action mechanisms of these chemicals are different from the action mechanisms of the anticancer drugs. However, we found that cisplatin did not belong to the cluster A, which consisted of DNA-targeting anticancer drugs. We do not understand the reason at present. However, there is a possibility that cisplatin has other action mechanisms, which may have made the fingerprint of cisplatin different from those of other DNA-targeting drugs. Indeed, cisplatin is known to form DNA-protein cross-links (Zwelling et al., 1979; Chválová et al., 2007).

Our analysis also identified several interesting clusters. For example, the cluster F3 consisted of cardiac glycosides digoxin and ouabain, both of which inhibit Na-K ATPase (Reuter et al., 2002). The cluster D1 consisted of 9-*cis* retinoic acid, 13-*cis* retinoic acid, and 4-[*E*-2-(5,6,7,8-tetrahydro-5,5,8,8-tetra-methyl-2-naphthalenyl)-1-propenyl]benzoic acid, which are RAR agonists. These results suggest that chemicals other than the anticancer drugs also form clusters when they share the same action mechanisms. It is noteworthy that SV-NNK and SV-NN, from snakes that belonged to the elapidae family, formed one cluster (cluster D2). In contrast, the snake venoms from the *C. atrox* and *T. flavoviridis*, which belonged to the viperidae family, formed a cluster (cluster D3) different from the elapidae cluster. These results are reasonable because snake venoms from different snake families are known to differ not only in composition but also in levels of toxicity and mechanisms of action.

The agricultural chemicals paraquat, ziram, and thiram were also classified into a single cluster (cluster F1). Among these agricultural chemicals, the action mechanism of ziram is not known. However, both paraquat and thiram are known to induce oxidative stress (Cereser et al., 2001; Suntres, 2002). Therefore, based on our observations, we could suggest that ziram also acted by inducing oxidative stress. The agricultural chemicals methoprene (insect growth regulator) and carbaryl (chorine esterase inhibitor) formed cluster L3, although their common mechanism is unknown. Cluster D4 and D5 consist of the antibacterial agents or fungicides. 3-Iodo-2-propynyl-butylcarbamate and *p*-chlorophenyl-3′-iodopropargylformal, belonging to cluster D4, are the iodo-type antibacterial agents.

Thus, cluster analysis of GI50 values of various chemicals, determined using the JFCR39 cell panel, suggests that the JFCR39 system could, at least in part, allow classification of chemical compounds on the basis of their action mechanisms. Our analysis also suggests that the chemicals belonging the same cluster share a common action mechanism. We are going to develop a larger library of reference chemicals with known action mechanisms (i.e., various inhibitors of biological pathways), and expand our database by integrating their GI50 measurements, which will make the cluster analysis as well as the COMPARE analysis more informative for predicting the mechanism of test chemicals.

In conclusion, to evaluate the potential of the JFCR39 system in predicting the action mechanisms of toxic chemicals, we investigated the fingerprints of 130 different types of chemical compounds including toxic chemicals, pesticides, drugs, and synthetic intermediates. Using the hierarchical clustering analysis, we classified 69 chemicals, at least in part, based on their action mechanisms. Thus, this approach using the JFCR39 cell panel is useful not only in predicting the action mechanisms of toxic chemicals but also in evaluating their toxicity.

Acknowledgments

We thank Yumiko Mukai, Yumiko Nishimura, and Mariko Seki for determination of chemosensitivity and Satoshi Kitajima for help with chemical information.

References

Akashi T, Nishimura Y, Wakatabe R, Shiwa M, and Yamori T (2007) Proteomics-based identification of biomarkers for predicting sensitivity to a PI3-kinase inhibitor in cancer. *Biochem Biophys Res Commun* **352:**514–521.

Akashi T and Yamori T (2007) A novel method for analyzing phosphoproteins using SELDI-TOF MS in combination with a series of recombinant proteins. *Proteomics* **7:**2350–2354

Aström A, Pettersson U, Krust A, Chambon P, and Voorhees JJ (1990) Retinoic acid and synthetic analogs differentially activate retinoic acid receptor dependent transcription. *Biochem Biophys Res Commun* **173:**339–345.

Cereser C, Boget S, Parvaz P, and Revol A (2001) An evaluation of thiram toxicity on cultured human skin fibroblasts. *Toxicology* **162:**89–101.

Chválová K, Brabec V, and Kasparkova J (2007) Mechanism of the formation of DNA-protein cross-links by antitumor cisplatin. *Nucleic Acids Res* **35:**1812–1821.

Dan S, Shirakawa M, Mukai Y, Yoshida Y, Yamazaki K, Kawaguchi T, Matsuura M, Nakamura Y, and Yamori T (2003) Identification of candidate predictive markers of anticancer drug sensitivity using a panel of human cancer cell lines. *Cancer Sci* **94:**1074–1082.

Dan S, Tsunoda T, Kitahara O, Yanagawa R, Zembutsu H, Katagiri T, Yamazaki K, Nakamura Y, and Yamori T (2002) An integrated database of chemosensitivity to 55 anticancer drugs and gene expression profiles of 39 human cancer cell lines. *Cancer Res* **62:**1139–1147.

Hershberger LG, Shipley EG, and Meyer RK (1953) Myotrophic activity of 19-nortestosterone and other steroids determined by modified levator ani muscle method. *Proc Soc Exp Biol Med* **83:**175–180.

Jamieson ER and Lippard SJ (1999) Structure, Recognition, and Processing of Cisplatin-DNA Adducts. *Chem Rev* **99:**2467–2498.

Kanno J, Kato H, Iwata T, and Inoue T (2002) Phytoestrogen-low diet for endocrine disruptor studies. *J Agric Food Chem* **50:**3883–3885.

Naasani I, Seimiya H, Yamori T, and Tsuruo T (1999) FJ5002: a potent telomerase inhibitor identified by exploiting the disease-oriented screening program with COMPARE analysis. *Cancer Res* **59:**4004–4011.

Nakamura H, Dan S, Akashi T, Unno M, and Yamori T (2007) Absolute quantification of four isoforms of the class I phosphoinositide-3-kinase catalytic subunit by real-time RT-PCR. *Biol Pharm Bull* **30:**1181–1184.

Nakatsu N, Yoshida Y, Yamazaki K, Nakamura T, Dan S, Fukui Y, and Yamori T (2005) Chemosensitivity profile of cancer cell lines and identification of genes determining chemosensitivity by an integrated bioinformatical approach using cDNA arrays. *Mol Cancer Ther* **4:**399–412.

Okutsu J, Tsunoda T, Kaneta Y, Katagiri T, Kitahara O, Zembutsu H, Yanagawa R, Miyawaki S, Kuriyama K, Kubota N, et al. (2002) Prediction of chemosensitivity for patients with acute myeloid leukemia, according to expression levels of 28 genes selected by genome-wide complementary DNA microarray analysis. *Mol Cancer Ther* **1:**1035–1042.

Paull KD, Shoemaker RH, Hodes L, Monks A, Scudiero DA, Rubinstein L, Plowman J, and Boyd MR (1989) Display and analysis of patterns of differential activity of drugs against human tumor cell lines: development of mean graph and COMPARE algorithm. *J Natl Cancer Inst* **81:**1088–1092.

Reuter H, Henderson SA, Han T, Ross RS, Goldhaber JI, and Philipson KD (2002) The Na^+-Ca^{2+} exchanger is essential for the action of cardiac glycosides. *Circ Res* **90:**305–308.

Scherf U, Ross DT, Waltham M, Smith LH, Lee JK, Tanabe L, Kohn KW, Reinhold WC, Myers TG, Andrews DT, et al. (2000) A gene expression database for the molecular pharmacology of cancer. *Nat Genet* **24:**236–244.

Suntres ZE (2002) Role of antioxidants in paraquat toxicity. *Toxicology* **180:**65–77.

Weinstein JN, Kohn KW, Grever MR, Viswanadhan VN, Rubinstein LV, Monks AP, Scudiero DA, Welch L, Koutsoukos AD, and Chiausa AJ (1992) Neural computing in cancer drug development: predicting mechanism of action. *Science* **258:**447–451.

Weinstein JN, Myers TG, O'Connor PM, Friend SH, Fornace AJ Jr, Kohn KW, Fojo T, Bates SE, Rubinstein LV, Anderson NL, et al. (1997) An information-intensive approach to the molecular pharmacology of cancer. *Science* **275:**343–349.

Wong E and Giandomenico CM (1999) Current status of platinum-based antitumor drugs. *Chem Rev* **99:**2451–2466.

Yaguchi S, Fukui Y, Koshimizu I, Matsuno T, Gouda H, Hirono S, Yamazaki K, and Yamori T (2006) Antitumor activity of ZSTK474, a new phosphatidyl inositol 3-kinase inhibitor. *J Natl Cancer Inst* **98:**545–556.

Yamori T (2003) Panel of human cancer cell lines provides valuable database for drug discovery and bioinformatics. *Cancer Chemother Pharmacol* **52 (Suppl 1):** S74–S79

Yamori T, Matsunaga A, Sato S, Yamazaki K, Komi A, Ishizu K, Mita I, Edatsugi H, Matsuba Y, Takezawa K, et al. (1999) Potent antitumor activity of MS-247, a novel DNA minor groove binder, evaluated by an in vitro and in vivo human cancer cell line panel. *Cancer Res* **59:**4042–4049,.

Zembutsu H, Ohnishi Y, Tsunoda T, Furukawa Y, Katagiri T, Ueyama Y, Tamaoki N, Nomura T, Kitahara O, Yanagawa R, et al. (2002) Genome-wide cDNA microarray screening to correlate gene expression profiles with sensitivity of 85 human cancer xenografts to anticancer drugs. *Cancer Res* **62:**518–527.

Zwelling LA, Anderson T, and Kohn KW (1979) DNA-protein and DNA interstrand cross-linking by cis- and trans-platinum(II) diamminedichloride in L1210 mouse leukemia cells and relation to cytotoxicity. *Cancer Res* **39:**365–369.

Address correspondence to: Takao Yamori, Division of Molecular Pharmacology, Cancer Chemotherapy Center, Japanese Foundation for Cancer Research, 3-10-6, Ariake, Koto-ku, Tokyo 135-8550, Japan. E-mail: yamori@jfcr.or.jp, 07a$sl

ELSEVIER

Experimental Hematology

Experimental Hematology 35 (2007) 1190–1200

Glycolytic inhibition by mutation of pyruvate kinase gene increases oxidative stress and causes apoptosis of a pyruvate kinase deficient cell line

Ken-ichi Aisaki[a], Shin Aizawa[b], Hisaichi Fujii[c], Jun Kanno[a], and Hitoshi Kanno[c,d,e]

[a]*Cellular and Molecular Toxicology Division, National Institute of Health and Sciences, Tokyo, Japan;* [b]*Department of Anatomy, Nihon University School of Medicine, Tokyo, Japan;* [c]*Department of Transfusion Medicine and Cell Processing;* [d]*Institute of Medical Genetics; and* [e]*Division of Genomic Medicine, Department of Advanced Biomedical Engineering and Science, Graduate School of Medicine, Tokyo Women's Medical University, Tokyo, Japan*

(Received 13 November 2006; revised 8 May 2007; accepted 9 May 2007)

Objective. **SLC3 is a Friend erythroleukemic cell line established from the *Pk-1*^{slc} mouse, a mouse model of red blood cell type-pyruvate kinase (R-PK) deficiency. This study was aimed to elucidate the mechanisms attributing to apoptosis induced by R-PK deficiency.**

Materials and Methods. **SLC3 and a control Friend cell line, CBA2, were cultured in a condition of glucose deprivation or supplementation with 2-deoxyglucose, and apoptosis was detected by annexin V. We established two stable transfectants of SLC3 cells with human R-PK cDNA, and examined the effect of R-PK on an apoptotic feature by cell cycle analysis. Intracellular oxidation was measured with 2′,7′-dichlorofluorescin diacetate. DNA microarray analysis was performed to examine gene-expression profiles between the two transfectants and parental SLC3.**

Results. **SLC3 was more susceptible than CBA2 to apoptosis induced by glycolytic inhibition. The forced expression of R-PK significantly decreased cells at the sub G_0/G_1 stage in an expression-level dependent manner. Microarray analysis showed that proapoptotic genes, such as *Bad*, *Bnip3*, and *Bnip3l*, were downregulated in the transfectants. In addition, peroxiredoxin 1 (*Prdx1*) and other antioxidant genes, such as *Cat*, *Txnrd1*, and *Glrx1* were also downregulated. A significant decrease of dichlorofluorescein fluorescence was observed by R-PK expression. Preincubation with a glutathione precursor showed a significant decrease of apoptosis.**

Conclusion. **These results indicated that glycolytic inhibition by R-PK gene mutation augmented oxidative stress in the Friend erythroleukemia cell, leading to activation of hypoxia-inducible factor-1 as well as downstream proapoptotic gene expression. Thus, R-PK plays an important role as an antioxidant during erythroid differentiation.** **© 2007 ISEH - Society for Hematology and Stem Cells. Published by Elsevier Inc.**

Glycolysis is an essential metabolic pathway in all organisms. Pyruvate kinase (PK) is a key glycolytic enzyme, and has four isoenzymes in mammals, designated M_1, M_2, L (liver), and R (red blood cell). In humans, these isozymes are encoded by two structural genes, *PKM* and *PKLR*, respectively [1]. M_2-PK is the only isozyme that is active in early fetal tissues and also almost ubiquitously expressed in adult tissues, including hematopoietic stem cells, progenitors, leukocytes, and platelets. Red blood cell type-pyruvate kinase (R-PK) becomes a major isozyme during erythroid differentiation/maturation [2,3], and in mature red blood cells (RBCs), R-PK is the only detectable PK isozyme. Deficiency of R-PK causes shortened RBC survival, resulting in hemolytic anemia. In humans, PK deficiency is the most prevalent glycolytic enzyme defect, which is responsible for hereditary hemolytic anemia [4,5].

We have previously established SLC3 [6], a line of Friend erythroleukemic cells from the *Pk-1*^{slc} mouse [7], which has chronic hemolytic anemia with marked splenomegaly due to a missense mutation of the murine *Pklr* gene [8]. SLC3 showed spontaneous apoptosis during routine passage and in vitro erythroid differentiation by butyrate exacerbated apoptosis of SLC3 [6]. Recently, we examined the spleen of a subject with severe PK deficiency [9], and discovered enhanced extramedullary hematopoiesis as well as apoptotic erythroid cells. Enhanced apoptosis

Offprint requests to: Hitoshi Kanno, M.D. Ph.D., Department of Transfusion Medicine and Cell Processing, Tokyo Women's Medical University, Tokyo 162-8666, Japan.

0301-472X/07 $–see front matter.
doi: 10.1016/j.exphem.2007.05.005

was also identified in TER119-positive erythroid cells isolated from *Pk-1*^{slc} mice [10]. These results provide evidence that the metabolic disturbances in PK deficiency affect not only the survival of RBCs but also the maturation of erythroid progenitors, which results in apoptosis.

In this study, we examined whether Friend erythroleukemic cell lines showed apoptosis when glycolysis was inhibited. To evaluate whether overexpression of the normal R-PK gene ameliorated apoptosis, we established stable transfectants of SLC3 and compared their apoptotic characteristics and transcriptional profiles with parental SLC3. We present here several pieces of evidence, revealing the biological significance of R-PK to suppress oxidative stress during erythroid differentiation.

Materials and methods

Cell culture and flow cytometric analysis

Friend erythroleukemic cell lines SLC3 and CBA2 have been described previously [6]. Both cell lines are maintained in Iscove's modified Dulbecco's medium (Invitrogen, Carlsbad, CA, USA) supplemented with 10% heat-inactivated fetal calf serum, 20 μM 2-mercaptoethanol, and a mixture of penicillin-streptomycin (Sigma-Aldrich, St Louis, MO, USA).

To evaluate the adverse effects of glycolytic inhibition, cells were cultured in either glucose-free RPMI-1640 (Invitrogen) or RPMI-1640 with 2-deoxyglucose (2-DG) at final concentrations of 0.1, 1, and 10 mM. Iscove's modified Dulbecco's medium containing 110 mg/L sodium pyruvate, and RPMI-1640 containing no pyruvate.

Flow cytometric analysis was performed by EPICS XL and analyzed with software, EXPO32 ADC (Beckman-Coulter, Fullerton, CA, USA). Annexin V-Alexa568 and rhodamine 123 were obtained from Roche Diagnostics (Basel, Switzerland) and Sigma, respectively. To examine the effect of N-acetyl-L-cysteine upon apoptosis, we preincubated cells in RPMI-1640 supplemented with 10 mM N-acetyl-L-cysteine for 12 hours, followed by 12- to 24-hour incubation with RPMI-1640.

Establishment of stable transfectants expressing normal R-PK in SLC3 cells

We constructed a human R-PK cDNA expression plasmid vector in erythroid cells. A 1.7-kb fragment covering the entire coding region of human R-PK cDNA [11] was introduced into *Kpn*I-*Eco*RV sites of pcDNA3.1 (Invitrogen). Plasmid DNA was purified with an EndoFree Maxi DNA purification kit (Qiagen, Hilden, Germany). Transfection was done with Effectene Transfection Reagent (Qiagen) as indicated by the manufacturer. Transfected cells were selected using G418 (400 μg/mL).

RT-PCR, Western blotting, and enzyme assay

Total cellular RNA was extracted with an RNeasy purification kit (Qiagen), and 2 μg RNA was reverse-transcribed (RT) at 42°C for 90 minutes with 50 pmole oligo (dT)17 primer, 0.5 U/μL cloned RNase inhibitor (Takara Bio, Shiga, Japan), 10 mM dithiothreitol, 1 mM deoxyribonucleoside triphosphate, and 50 U Expand Reverse Transcriptase (Roche Diagnostics). Aliquots (1/10) were subjected to PCR using primer pairs specifically amplified with human and murine R-PK cDNA, hRPK-F (5′-TGGCCCAGC CTACCCTTGTA-3′)/hRPK-R (5′-CTTAAAGGTGGGGCTTTG GA-3′) and mRPK-F (5′-GCAGATGATGTGGACCGAAG-3′)/ mRPK-R (5′-CTAGATGGCAGATGTGGGACTA-3′), respectively. The reaction mixtures were subjected to 40 cycles of amplification consisting of 94°C for 20 seconds, 60°C for 10 seconds, and 72°C for 10 seconds for hRPK and 94°C for 20 seconds, 60°C for 20 seconds, and 72°C for 20 seconds for mRPK in a GeneAmp PCR system 2400 (Roche Diagnostics, Switzerland), and separated using 2% agarose gel electrophoresis.

For Western blot analysis, cells were harvested, followed by washing with phosphate-buffered saline twice. Following three-times freezing and thawing in extraction buffer (10 mM Tris/HCl, pH 8.0, 10 mM $MgCl_2$, 0.003% 2-mercaptoethanol, 0.02 mM ethylenediamine tetraacetic acid), cell extracts were obtained for Western blot analysis. Protein assays were performed by the method of Bradford using a commercial kit (Bio-Rad Laboratories, Hercules, CA, USA).Western blot analysis was conducted using anti-rat L-PK (kindly provided Tamio Noguchi, Nagoya University) and ECL advance Western Blotting Detection Kit (Amersham Biosciences, Buckinghamshire, UK).

PK and lactate dehydrogenase (LDH) activity was measured, as described [12].

Microarray analysis

To prepare high-quality total cellular RNA for the GeneChip assay, RNA was extracted with modified protocols using the TRIzol LS (Invitrogen) and RNeasy purification kit (Qiagen). Briefly, cells were harvested with no washing step, and immediately homogenized with the RLT buffer. The lysate was then mixed with 3 volumes of the TRIzol LS. After a 10-minute incubation at room temperature, the sample solution was mixed with an equal volume of chloroform. The sample was centrifuged at 10,000*g* for 15 minutes at 4°C, and then the upper aqueous phase was transferred to a fresh tube. After mixing with an equal volume of 70% ethanol, the sample was incubated for 10 minutes at room temperature. Without any flash step, the sample solution was transferred to the RNeasy column, and then processed by the manufacturer recommended protocol.

To normalize the variation in data based on the cell count, we used *Bacillus subtilis* RNA for an external standard signal, which was added to the cell lysate in proportion to the sample's DNA contents [13]. Ten microliters of cell lysate was provided for DNA quantification using Picogreen (Invitrogen). GeneChip (Affymetrix, Santa Clara, CA, USA) analysis was carried out according to the Affymetrix-recommended protocols. Processed RNA was hybridized to the Affymetrix Murine Genome 430A arrays (22960 probe sets). Signal values were calculated from scanned images by the Affymetrix Microarray Operation System (GCOS). The cell sample was pooled from six culture dishes at each condition and one GeneChip was used per one pooled sample.

Data analysis

Data were normalized by an original program (SCal), which processes data in proportional conversion based on the DNA content of each biosample [13]. This DNA content-based normalization method improves the measurement accuracy of GeneChip. For example, a series of samples was measured by quantitative PCR and Affymetrix GeneChip microarrays using this method, and the results showed up to 90% concordance [13].

To identify differentially expressed genes, we used an empirical threshold calculated by an original algorithm (Fx). The Fx threshold is based on the signal intensity level and is calculated as follows: $Y = X \cdot (1 + RC^{(w\text{-}\log X)})$ and $Y = X \cdot (1 + C^{(w\text{-}\log X)})^{-1}$ (Fx1 and Fx2 respectively; C and w are constant parameters reflecting actual measurement data by GeneChip hybridized with the standard sample). C and w were set to 3.0 and 2.5, respectively, which was equivalent to $p < 0.02$. In the scatter plot, the spots above the Fx1 line were evaluated as upregulated, and the spots below the Fx2 line were evaluated as downregulated.

Results

SLC3 is more susceptible than the control to apoptosis due to glycolytic inactivation

Figure 1 shows flow cytometric analysis using annexin V (horizontal axis) and rhodamine 123 (vertical axis) to examine the effects of glycolysis inhibition on Friend leukemic cells with or without R-PK mutation. SLC3 showed spontaneous apoptosis during routine passage, and apoptosis preceded mitochondrial dysfunction in the R-PK–deficient erythroleukemia cells as reported previously [6]. The result showed that a part of apoptotic cells kept similar mitochondrial transmembrane potentials and that SLC3 were much more susceptible to glucose deprivation as well as 2-DG.

Overexpression of wild-type R-PK decreases apoptosis of SLC3

In order to evaluate how wild-type R-PK rescues apoptotic phenotypes, we established two stable transfectants of SLC3 with overexpression of the human R-PK cDNA. Figure 2 shows RT-PCR and Western blot analysis of a parental SLC3 and SLC3-hRPK.Hi (hRPK.Hi) and SLC3-hRPK.Lo (hRPK.Lo). As shown in Figure 2A, the expression level of the transgene was higher in hRPK.Hi than hRPK.Lo. Overexpression of human R-PK suppressed endogenous R-PK expression as observed in the lane of hRPK.Hi.

Enzymatic analysis of transfectants revealed that PK activities of hRPK.Lo and Hi were 17.2 and 24.2 IU/mg protein, respectively. The PK activity of hRPK.Hi was almost comparable to parental SLC3, 23.5 IU/mg protein. It should be noted that endogenous LDH activity was decreased by transgene expression, leading to a PK/LDH ratio increase from 0.4 (SLC3) to 0.48 (hRPK.Lo) and 0.6 (hRPK.Hi).

We evaluated apoptosis of the two transfectants by cell cycle analysis. Figure 2C shows that the expression of wild-type R-PK decreased the number of cells at the sub-G_0/G_1 stage. While hRPK.Lo showed almost the same number of sub-G_0/G_1 cells (55.5%) as SLC3 (57.4%), only 19.3% of hRPK.Hi were arrested at the sub G_1-stage. Because apoptotic cells were rescued from apoptosis in an R-PK expression level-dependent manner, it is most likely that R-PK activity is required to suppress apoptosis of erythroid cells.

Microarray analysis elucidates the differential expression of genes involved in reactive oxygen species removal, cell cycle, and apoptosis

Gene expression profiles between the two transfectants and the parental SLC3 cell line were analyzed by DNA microarray analysis. After exchanging culture medium, SLC3, hRPK.Lo, and Hi were sampled at 24 and 67 hours, which were the phase of reentry into cell cycling and of subconfluence, respectively. Transgene expression upregulated only about 2% (469 probe sets) of genes, whereas approximately 25% (5754 probe sets) of genes were downregulated both in hRPK.Hi and hRPK.Lo at 24 and/or 67hours. As shown in Figure 3B, major categories of the downregulated genes involved the cell cycle, development, and apoptosis. Proapoptotic genes including *Bad*, *Bnip3*, and *Bnip3l*, as well as *Casp 2, 6, 7,* and *8* were downregulated (Figs. 3A and 4).

Genes of key glycolytic enzymes such as hexokinase-2 (*Hk2*), phosphofructokinase (*Pfkl*), phosphoglycerate kinase (*Pgk1*), and PK (*Pklr*) were downregulated, and expression levels were characteristically decreased after 67 hours of transfection, suggesting that suppression requires protein synthesis.

It should be noted that genes for antioxidant protein, such as peroxiredoxin 1 (*Prdx1*) and related genes, such as catalase (*Cat*), thioredoxin reductase 1 (*Txnrd1*), and glutaredoxin 1 (*Glrx1*), which have a role in the modulation of oxidative stress, are also downregulated. As for *Prdx2*, expression change by the transgene was not evident. Intracellular reactive oxygen species (ROS) are known to cause DNA damage, inducing the expression of DNA repair genes. In this experiment, expressions of genes involved in DNA repair were decreased, including *Brca1*, *Brca2*, and *Rad51*.

PK gene mutation and glycolytic inhibition by 2-DG augment intracellular ROS

We examined intracellular ROS in SLC cells and control CBA2 cells by 2′,7′-dichlorofluorescin-diacetate (DCFH-DA), an indicator of the intracellular formation of hydrogen peroxide and free radicals. Nonfluorescent DCFH-DA turns into DCFH (2′,7′-dichlorofluorescin) in the presence of hydrogen peroxide, and then DCFH is quickly photo-oxidized to fluorescent DCF (2′,7′-dichlorofluorescein).

Figure 5A shows that SLC3 is hypersensitive to a glycolytic inhibitor, 2-DG, producing intracellular DCF by adding 1 mM 2-DG. In contrast, control CBA2 cells do not produce DCF even at 10 mM 2-DG for 30 minutes.

Reduced glutathione (GSH) is an important antioxidant in erythrocytes. GSH is produced by a two-step enzymatic reaction involving γ-glutamylcystein synthetase and glutathione synthetase (GSH-S). Apoptosis induced either by the glycolytic gene mutation (SLC3) or the glycolytic inhibitor (CBA with 2-DG) was suppressed by preincubation with the glutathione precursor, NAC (Fig. 5B). Finally, the

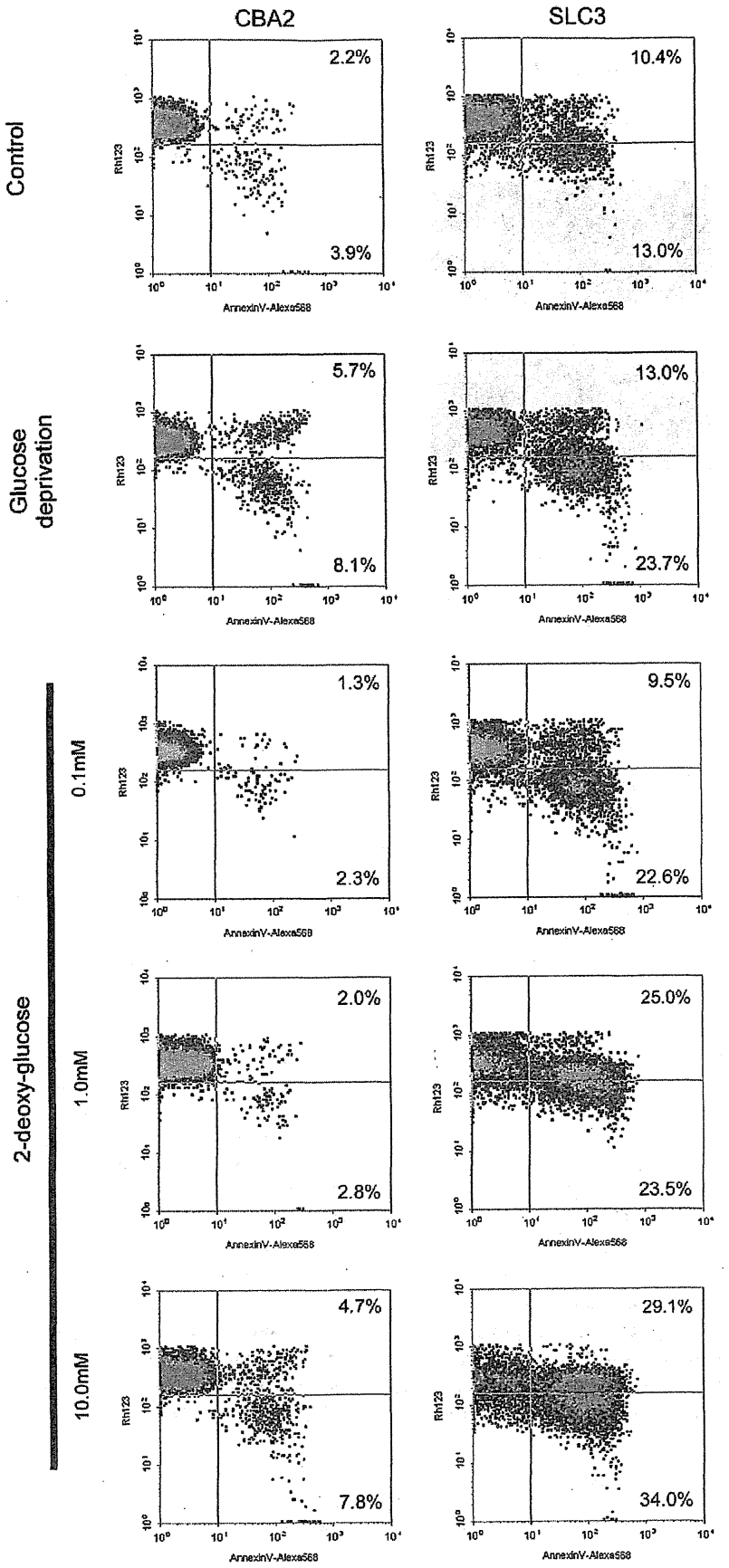
CBA2
SLC3
Control
Glucose deprivation
2-deoxy-glucose
0.1mM
1.0mM
10.0mM
2.2%
3.9%
10.4%
13.0%
5.7%
8.1%
13.0%
23.7%
1.3%
2.3%
9.5%
22.6%
2.0%
2.8%
25.0%
23.5%
4.7%
7.8%
29.1%
34.0%
Rh123
AnnexinV-Alexa568

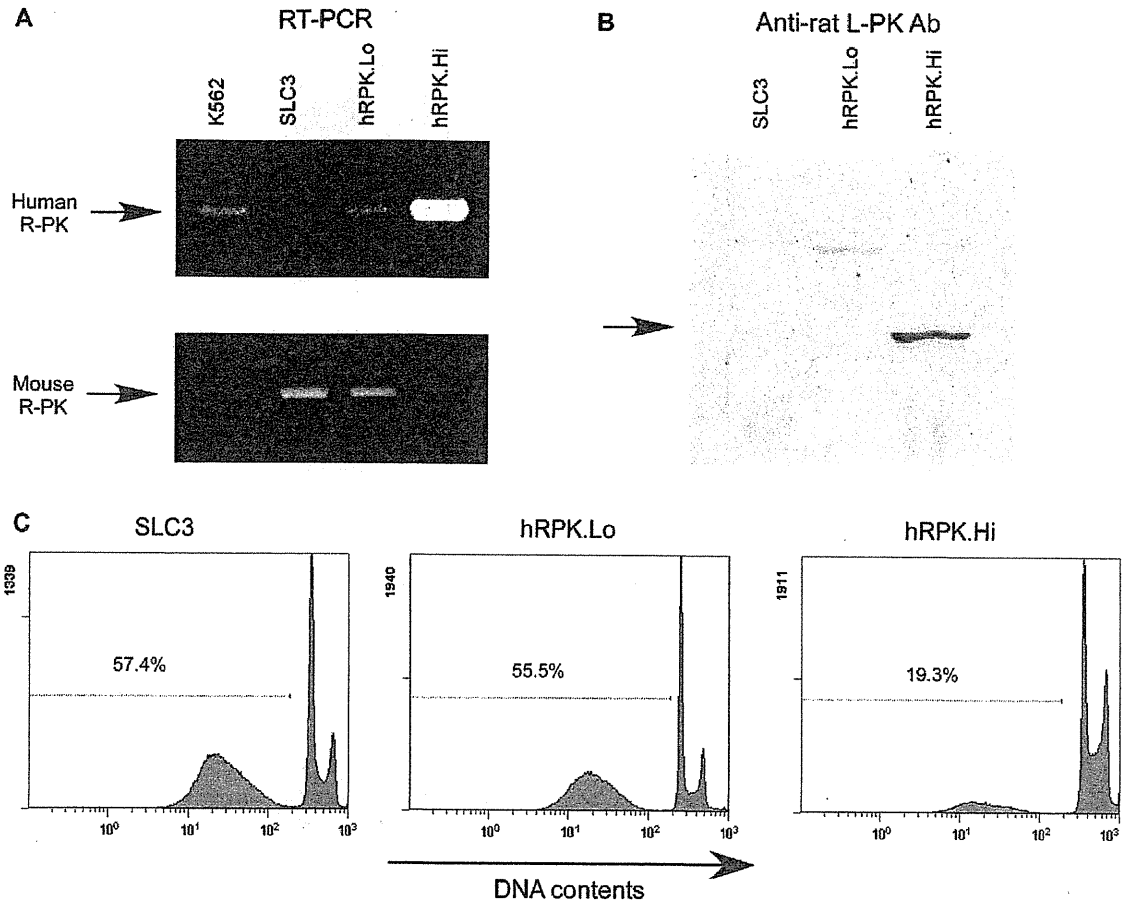

Figure 2. Establishment of the transfectants, SLC3-hRPK.Hi (hRPK.Hi) and SLC3.hRPK.Lo (hRPK.Lo), by introducing the human red blood cell type-pyruvate kinase (R-PK) gene into murine R-PK–deficient cells. Transgene-expression was confirmed by reverse transcriptase polymerase chain reaction (**A**) and Western blotting (**B**). The expression level of hRPK.Hi was higher than that of hRPK.Lo. (**C**) Apoptosis induction in the PK-deficient cells and transfectants. Transfected human R-PK recovered the glycolytic function and showed reduced spontaneous apoptotic changes. The numbers in figures represent the apoptotic change ratio.

forced overexpression of the PK gene reduced intracellular ROS in an expression-level dependent manner (Fig. 5C).

Discussion

Overexpression of human R-PK in SLC3 results in the reduction of apoptotic cells (Fig. 2C), and DNA microarray analysis showed that genes involved in the cell cycle, DNA repair, and antioxidants were downregulated. In general, gene expression levels of transfectants were lower than that of SLC3 (Fig. 3). However, aberrant apoptosis and invalid cell proliferation were restrained in the transfectants. These observations suggested that the cellular activity was not suppressed but was reverted to the normal level by the transgene. It is most likely that the candidate genes suppressed in transfectants were induced in R-PK mutant cells.

Although there were several candidate genes attributing to apoptosis-induction in SLC3, it was still unclear whether these genes were associated with each other or independent. However, there was a possibility that a signal cross-talk phenomenon occurred [14]. *Bad*, a gene encoding a member of the Bcl2-family proapoptotic molecules in mitochondria was significantly downregulated by the transgene (Figs. 3A and 4). Danial et al. [15] reported that *Bad*, BCL2-antagonist of cell death, formed a functional holoenzyme complex together with several molecules, such as glucokinase (hexokinase-4) in liver mitochondria, and contributed to apoptosis induction by glucose deprivation. Our observation suggested that *Bad*

Figure 1. Apoptosis induced by glycolytic inhibition in erythroid cell lines. Glucose deprivation or exposure to 2-deoxyglucose inhibits glycolysis and finally causes apoptosis. The red blood cell type-pyruvate kinase (R-PK)–deficient erythroid cell line (SLC3) is more susceptible than wild-type cells (CBA2) in these conditions. The horizontal axis shows AnnexinV-Arexa568 (= apoptotic change) and the vertical axis shows Rhodamin123 fluorescence (= mitochondrial membrane potential).

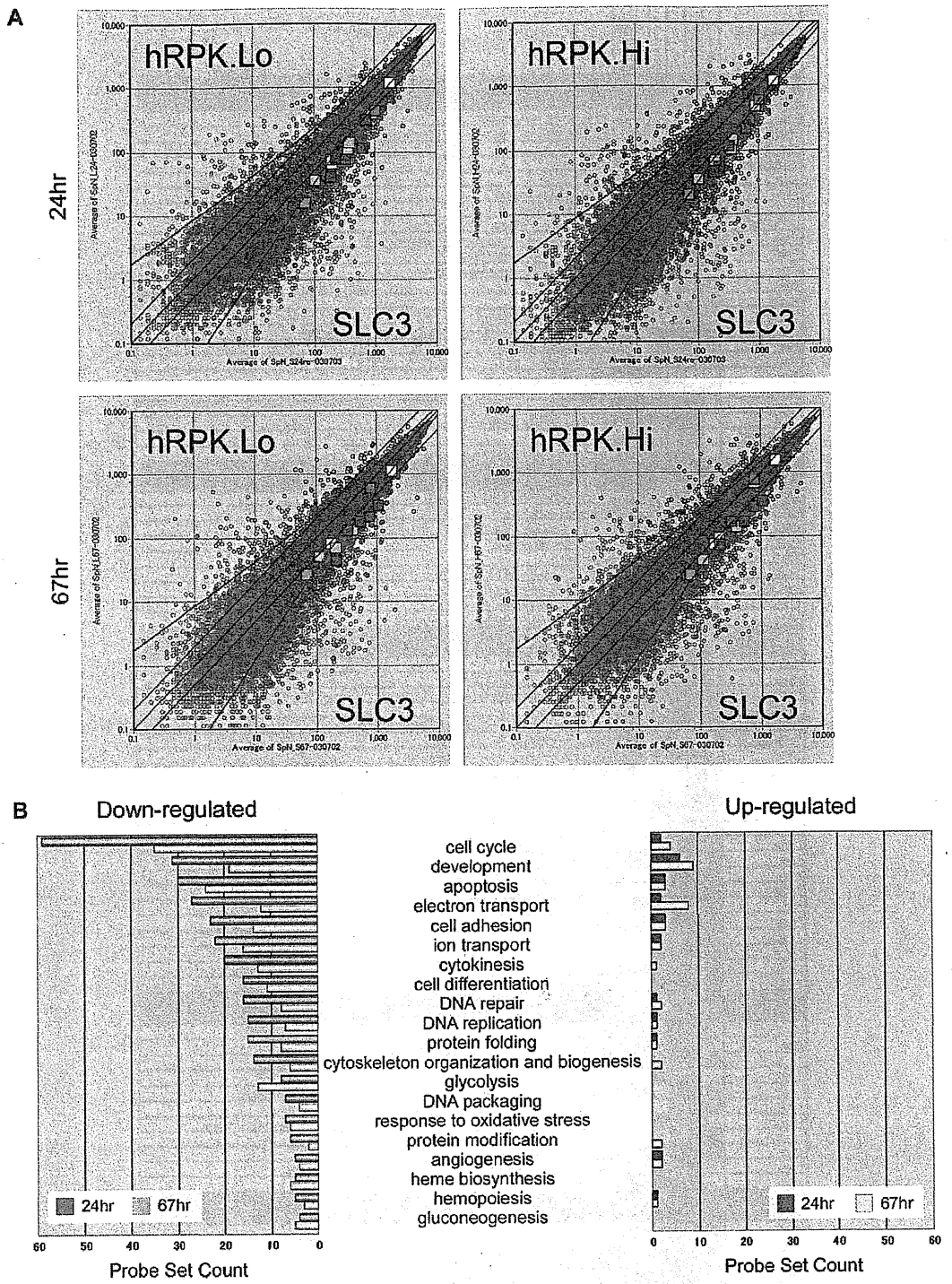

Figure 3. Genome-wide expression analysis of the glycolysis defect. Analysis was performed using the Affymetrix GeneChip Mouse Expression Array 430A, which contains about 20,000 genes. (**A**) Scatter plot between SLC3 and hRPK transfectants at 24 or 67 hours. The open circle shows the expression level of every probe set. The color shows these probabilities provided by the Affymetrix GeneChip Operation System: red means good and green means poor. The colored squares show *Bad* (red), *Bnip3* and *Bnip3l* (blue), *hif1a* (green), *Brca1* and *Brca2* (aqua), *Prdx1* (pink) and *Txnl1* (yellow), respectively. The black lines show twofold, onefold, and 0.5-fold, respectively, and the blue lines show the empirical threshold level. (**B**) The categorized aggregate graph. All probe sets were categorized by the Biological Process Ontology keywords provided by the Gene Ontology project (http://www.geneontology.org/). Up- or downregulation was determined by the spot location in the scatter plotting. Compared with the empirical threshold lines, the upper spots show upregulated genes and the lower spots show downregulated genes.

A Down-regulated Genes

Common Name	24hr SLC3	24hr hRPK.Lo	24hr hRPK.Hi	67hr SLC3	67hr hRPK.Lo	67hr hRPK.Hi	Description
apoptosis							
Bad							Bcl-associated death promoter
Bnip3l							BCL2/adenovirus E1B 19kDa-interacting protein 3-like
Casp7							caspase 7
Casp8							caspase 8
Cul7							Cullin 7
Hells							helicase, lymphoid specific
Ltbr							lymphotoxin B receptor
MGI:1353605							Cd27 binding protein (Hindu God of destruction)
P2rx1							purinergic receptor P2X, ligand-gated ion channel, 1
Plagl2							pleiomorphic adenoma gene-like 2
Sh3glb1							SH3-domain GRB2-like B1 (endophilin)
Brca1							breast cancer 1
Casp6							caspase 6
Casp8ap2							caspase 8 associated protein 2
Cdkn1a							cyclin-dependent kinase inhibitor 1A (P21)
Faf1							Fas-associated factor 1
Txnl1							thioredoxin-like 1
Bcl6							B-cell leukemia/lymphoma 6
Casp2							caspase 2
Dapk1							death associated protein kinase 1
Dsip1							delta sleep inducing peptide, immunoreactor
MGI:1915044							scotin gene
Tnfrsf1a							tumor necrosis factor receptor superfamily, member 1a
glycolysis							
Gpi1							glucose phosphate isomerase 1
Pgam1							phosphoglycerate mutase 1
Pklr							pyruvate kinase liver and red blood cell
Pgk1							phosphoglycerate kinase 1
Hk2							hexokinase 2
Eno1							enolase 1, alpha non-neuron
Ldh1							lactate dehydrogenase 1, A chain
Pfkl							phosphofructokinase, liver, B-type
Tpi1							triosephosphate isomerase 1
electron transport							
Cat							catalase
Cox8a							cytochrome c oxidase, subunit VIIIa
Glrx1							glutaredoxin 1 (thioltransferase)
Maoa							monoamine oxidase A
Ndufs7							NADH dehydrogenase (ubiquinone) Fe-S protein 7
Txnrd1							thioredoxin reductase 1
Uqcrc1							ubiquinol-cytochrome c reductase core protein 1
1110060M21Rik							RIKEN cDNA 1110060M21 gene
2410011G03Rik							RIKEN cDNA 2410011G03 gene
Acad8							acyl-Coenzyme A dehydrogenase family, member 8
Acad9							acyl-Coenzyme A dehydrogenase family, member 9
Cai							calcium binding protein, intestinal
Cox6a1							cytochrome c oxidase, subunit VI a, polypeptide 1
Cycs							cytochrome c, somatic
Ern1							endoplasmic reticulum (ER) to nucleus signalling 1
Fads2							fatty acid desaturase 2
Nxn							nucleoredoxin
Txndc1							thioredoxin domain containing 1
Txnl1							thioredoxin-like 1
Uqcrc2							ubiquinol cytochrome c reductase core protein 2
Cyba							cytochrome b-245, alpha polypeptide
Sdhb							succinate dehydrogenase complex, subunit B, iron sulfur (Ip)
response to stress							
Cat							catalase
Prnp							prion protein
Tacc3							transforming, acidic coiled-coil containing protein 3
Txnip							thioredoxin interacting protein
Ercc2							excision repair cross-complementing rodent repair deficiency, complementation group 2
Ern1							endoplasmic reticulum (ER) to nucleus signalling 1
Herpud1							homocysteine-inducible, endoplasmic reticulum stress-inducible, ubiquitin-like domain member 1
Prdx1							peroxiredoxin 1
Stip1							stress-induced phosphoprotein 1
Prkra							protein kinase, interferon inducible double stranded RNA dependent activator
Xpa							xeroderma pigmentosum, complementation group A
DNA repair							
Brca2							breast cancer 2
Cspg6							chondroitin sulfate proteoglycan 6
Ddb1							damage specific DNA binding protein 1
Fancl							Fanconi anemia, complementation group L
Fen1							flap structure specific endonuclease 1
Rad51							RAD51 homolog (S. cerevisiae)
Brca1							breast cancer 1
Csnk1d							casein kinase 1, delta
Ercc2							excision repair cross-complementing rodent repair deficiency, complementation group 2
Gtf2h4							general transcription factor II H, polypeptide 4
Rad23b							RAD23b homolog (S. cerevisiae)
Rad50							RAD50 homolog (S. cerevisiae)
Tdg							thymine DNA glycosylase
Mll							myeloid/lymphoid or mixed-lineage leukemia
Xpa							xeroderma pigmentosum, complementation group A

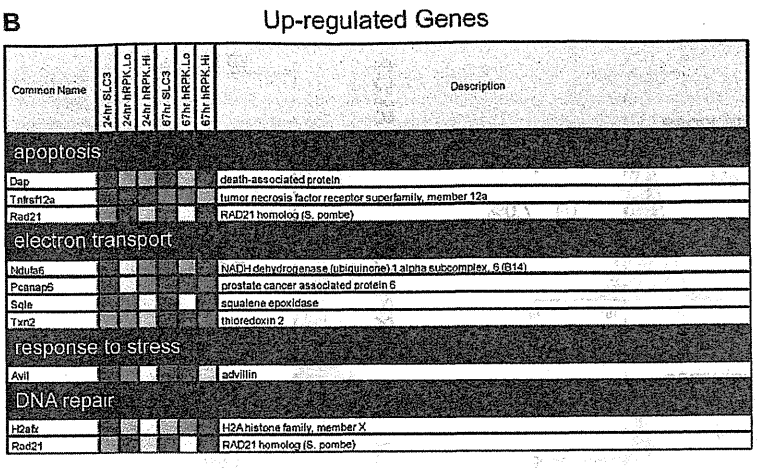

Figure 4. *Continued*

could be involved in the apoptosis induced by glycolysis defect in erythroid cells as well as in the liver.

The genes of apoptosis-inducers related to hypoxia such as *Bnip3* and *Bnip3l*, which are known as inducible genes by hypoxia-inducible factor-1α, were inactivated markedly by the forced expression of the wild-type R-PK gene. Although the extent of downregulation was smaller than for *Bnip3*, *Bnip3l* showed a significant decrease of expression by the transgene (Fig. 3A). Moreover, the downregulation was more obvious at 24 hours, suggesting that these genes may contribute to the initial response caused by a glycolytic defect. These observations strongly suggested that the apoptosis induction by the glycolysis disorder was executed by the *Bnip3-Bnip3l* signal.

It is noticeable that several genes important for responding to oxidative stress are upregulated, suggesting that R-PK deficiency might account for intracellular ROS production. This speculation is supported by the following experimental observations: Firstly, SLC3 cells were more sensitive to glycolytic inhibitions such as glucose deprivation and supplementation with 2-DG (Fig. 1), and these conditions induced ROS production detected by DCFH-DA (Fig. 5A). Apoptotic changes induced by 2-DG were partly rescued by preincubation with the glutathione precursor (Fig. 5B). Finally, transgene expression reduced intracellular ROS in an expression-level–dependent manner (Fig. 5C).

Glycolytic disorders may cause cellular conditions similar to those of hypoxia. Shim et al. [16] reported that induction of the LDH-A gene by c-Myc was advantageous to transformed cells that exist under hypoxic conditions [15]. However, glucose deprivation induces the extensive apoptosis of cells overexpressing c-Myc. Overexpression of LDH-A alone in fibroblasts is sufficient to sensitize cells to this glucose deprivation-induced apoptosis. They proposed a hypothesis that LDH-A was a downstream target of c-Myc that mediates this unique apoptotic phenotype. We noticed that pyruvate was the final product as well as the substrate of the PK and LDH reaction, respectively. Both LDH hyperactivity and PK deficiency may cause the depletion of intracellular pyruvate, suggesting that pyruvate has an important role in preventing apoptosis.

Several studies have revealed that pyruvate acts as an antioxidant and that PK has a protective role against oxidative stress in this respect. Brand et al. [17] reported that proliferating thymocytes mainly depend on energy derived from aerobic glycolysis, and that their sensitivity to 12-myristate 13-acetate–induced ROS production is much lower than that of resting thymocytes, which produce ATP mainly through oxidative phosphorylation. They suggested that pyruvate functions as an ROS scavenger, because the incubation of proliferating thymocytes with pyruvate reduced ROS formation.

The PK-overexpressing neuronal cells could attenuate oxidative stress and maintain cell viability [18]. Lee et al. [19] showed that hydrogen peroxide depleted intracellular GSH in human umbilical vein endothelial cells, and that was prevented by pyruvate but not by L-lactate or aminooxyacetate. The activation of caspases was strongly inhibited by pyruvate, but markedly enhanced by L-lactate and aminooxyacetate, implicating the redox-related antiapoptotic mechanisms of pyruvate. Myocardial ischemia-reperfusion

Figure 4. Representative list of the genes affected by the functional recovery of glycolysis. Genome-wide expression analysis was performed using Affymetrix GeneChip Mouse Expression Array 430A, which contains about 20,000 genes. In the comparison among hRPK.Hi, hRPK.Lo, and SLC3, about 6000 genes were downregulated and about 500 genes were upregulated by the functional recovery of glycolysis at 24 and/or 67 hours after regular passage. These lists contain the affected genes related to apoptosis and/or the oxidative stress response.

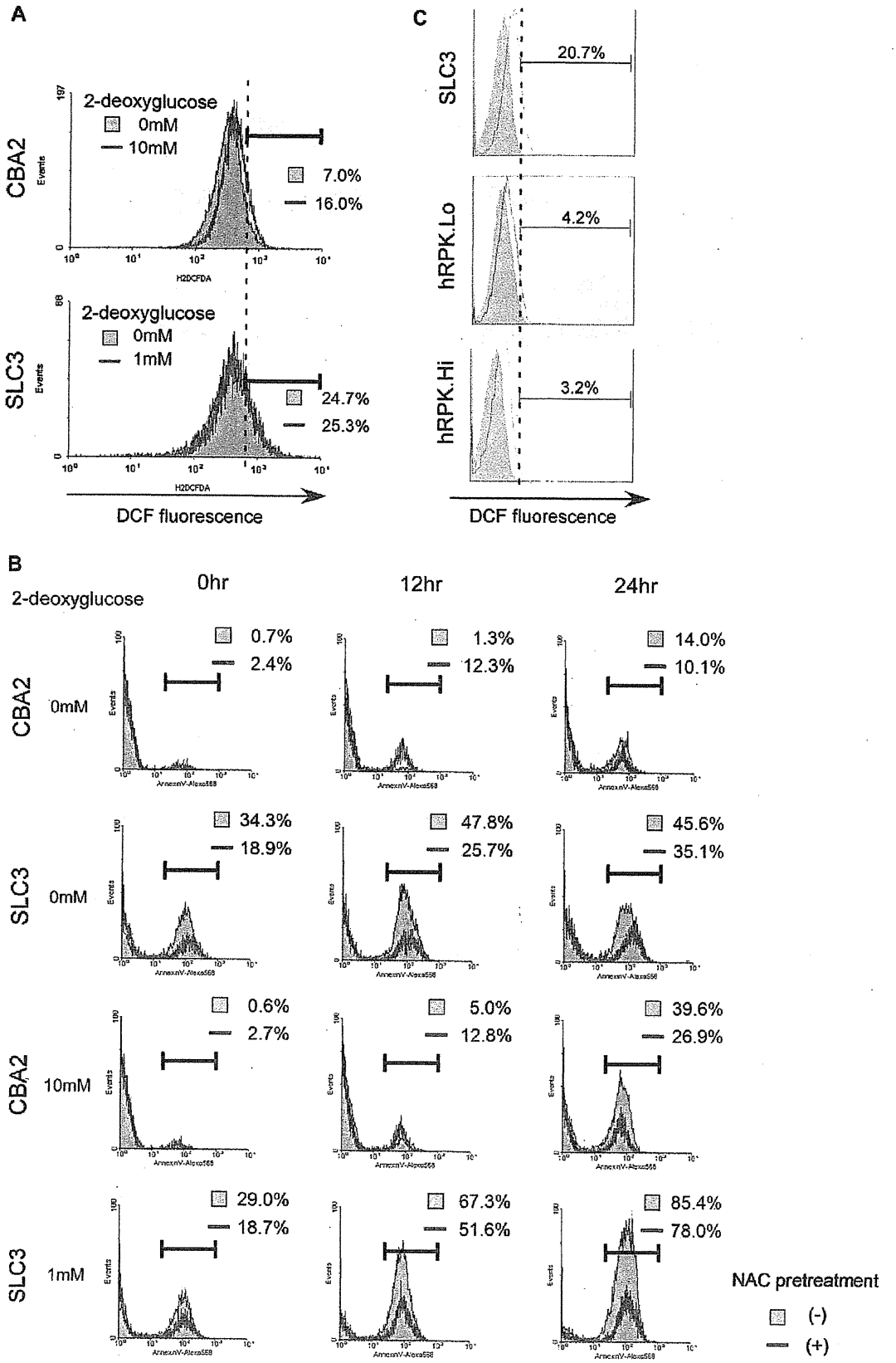
A
CBA2
2-deoxyglucose
0mM
10mM
7.0%
16.0%
SLC3
2-deoxyglucose
0mM
1mM
24.7%
25.3%
Events
H2DCFDA
DCF fluorescence
C
SLC3
20.7%
hRPK.Lo
4.2%
hRPK.Hi
3.2%
DCF fluorescence
B
2-deoxyglucose
0hr
12hr
24hr
CBA2 0mM
0.7% 2.4%
1.3% 12.3%
14.0% 10.1%
SLC3 0mM
34.3% 18.9%
47.8% 25.7%
45.6% 35.1%
CBA2 10mM
0.6% 2.7%
5.0% 12.8%
39.6% 26.9%
SLC3 1mM
29.0% 18.7%
67.3% 51.6%
85.4% 78.0%
AnnexinV-Alexa568
NAC pretreatment
(-)
(+)

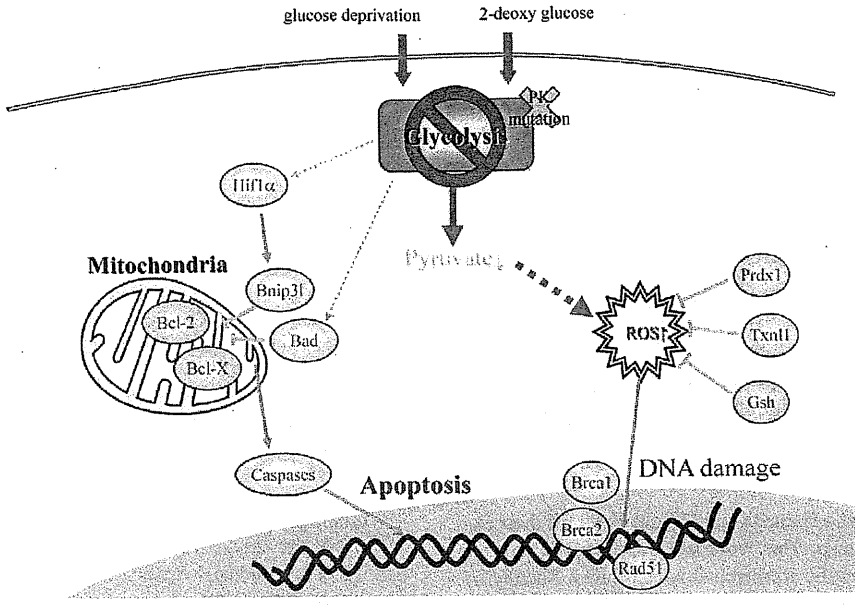

Figure 6. Glycolytic defect causes oxidative stress and hypoxia-like signal activation. Pyruvate, which is final metabolic product of the glycolytic pathway, acts as an antioxidant. Therefore, glycolytic defect elevates intracellular reactive oxygen species (ROS) and causes cellular damage, such as DNA damage and lipid oxidation. At the same time, glycolytic defect is most likely to activate signal transduction through hypoxia-inducible factor-1α (HIF-1α). These cellular responses could be accountable for the apoptosis induced by glycolytic defect.

is reported to be associated with bursts of ROS, such as superoxide radicals, and cardiac superoxide formation can be inhibited by pyruvate [20]. Thus cytotoxicities due to cardiac ischemia-reperfusion ROS can be alleviated by redox reactants such as pyruvate. These results support our present data, which showed that a mutation of the PK gene as well as inhibition of glycolysis by 2-DG augmented intracellular ROS of erythroid cells, leading to apoptosis. Introduction of the wild-type PK gene into SLC3 cells partly reduced ROS and apoptosis (Figs. 2C and 6C).

In human RBC, the most important antioxidant is GSH. Mutations of enzymes involving the synthesis and reduction of GSH, such as γ-glutamylcystein synthetase, GSH-S, glutathione reductase, and glucose-6-phosphate dehydrogenase account for the shortened RBC survival [1,21]. Recently, Neumann et al. [22] and Lee et al. [23] reported the essential roles of both peroxiredoxin (Prdx) 1 and 2 in RBC protection from oxidative stress. The hemolytic anemia of mice with targeted inactivation of *Prdx1* is characterized by an increase in erythrocyte reactive oxygen species, leading to protein oxidation and Heinz body formation. Similarly, the *Prdx2* knockout mice had Heinz body-positive hemolytic anemia with splenomegaly. The dense RBC fractions contained markedly higher levels of ROS. These studies highlighted a pivotal role of *Prdx* as a scavenger of hydrogen peroxide in RBC. *Prdx1* may be concerned with the initial response to glycolytic deficiency, because the gene expression in SLC3 was higher than that in transfectants only at 24 hours (Fig. 3A). The mechanisms responsible for upregulation of *Prdx1* and similar antioxidant enzymes in SLC3 remain to be elucidated.

It is most likely that the main pathogenesis of PK deficiency is decreased ATP production due to impaired glycolysis, resulting in the premature destruction of RBC in the reticuloendothelial system, i.e., extravascular hemolysis. In most cases, hemolysis is partly compensated by enhanced erythropoiesis. We have previously shown that the numbers of hematopoietic progenitors including colony-forming unit (CFU)-erythroid, CFU-granulocyte macrophage, burst-forming unit-erythroid, and CFU-granulocyte-erythrocyte monocyte-megakaryocyte were increased in *Pk-1*^{slc} mice [10]. The proliferation of erythroid progenitors might require

Figure 5. The oxidative stress pathway might play some role in the apoptosis induced by glycolytic disorder. (**A**) The SLC3 cells produce 2′,7′-dichlorofluorescein (DCF) continuously with and without 2-deoxyglucose (2-DG) due to the red blood cell type-pyruvate kinase (R-PK) defect. The control CBA2 cells produce DCF with 10 mM 2-DG for 30 minutes. The gray area shows the nontreated group and the red line shows the treated group with 2-DG. The horizontal axis shows the fluorescence intensity of the DCF. (**B**) The apoptosis induced by glycolytic defect or by glycolysis inhibitor was suppressed by the preincubation with the glutathione precursor, N-acetyl-cysteine (NAC). The gray area shows the nonpretreated group and the blue line shows the pretreated group with NAC. The horizontal axis shows the fluorescence intensity of the Annexin V-Alexa568.

activation of glycolysis in order to suppress intracellular ROS. Therefore, R-PK deficiency becomes a serious problem for erythroid cells to avoid apoptosis. In summary, we concluded that the premature destruction of RBC as well as apoptosis of erythroid progenitors accounts for the pathogenesis of R-PK deficiency.

Although most severe cases die either in utero or during the neonatal period [24,25], there is no curative therapy of PK deficiency except hematopoietic stem cell transplantation [26] at present. Because hematopoietic stem cell transplantation may accompany life-threatening complications, a safer treatment should be considered. Studies on the apoptotic induction of erythroid progenitors in R-PK deficiency may be useful for the identification of molecular targets of causal treatment.

Acknowledgments

We are indebted to Takako Hamada and Miyuki Yuda for their excellent technical assistance. This work was supported in part by a Grant-in-Aid for Scientific Research from the Japan Society of the Promotion of Science (project nos. 14570131 and 16590254), and also by a Scientific Research Grant from the Ministry of Health, Labor and Welfare (H15-kagaku-002, H18-kagaku-ippan-001), Japan.

References

1. Hirono A, Kanno H, Miwa S, Beutler E. Pyruvate kinase deficiency and other enzymopathies of the erythrocyte. In: Scriver CR, Beaudet AL, Sly WS, Valle D, eds. The Metabolic & Molecular Bases of Inherited Disease. 8th ed. New York: McGraw-Hill; 2001. p. 4637–4664.
2. Takegawa S, Fujii H, Miwa S. Change of pyruvate kinase isozymes from M2- to L-type during development of the RBC. Br J Haematol. 1983;54:467–474.
3. Max-Audit I, Kechemir D, Mitjavila MT, Vainchenker W, Rotten D, Rosa R. Pyruvate kinase synthesis and degradation by normal and pathologic cells during erythroid maturation. Blood. 1988;72: 1039–1044.
4. Tanaka KR, Zerez CR. RBC enzymopathies of the glycolytic pathway. Semin Hematol. 1990;27:165–185.
5. Zanella A, Fermo E, Bianchi P, Valentini G. RBC pyruvate kinase deficiency: molecular and clinical aspects. Br J Haematol. 2005;130: 11–25.
6. Aisaki K, Kanno H, Oyaizu N, Hara Y, Miwa S, Ikawa Y. Apoptotic changes precede mitochondrial dysfunction in red cell-type pyruvate kinase mutant mouse erythroleukemia cell lines. Jpn J Cancer Res. 1999;90:171–179.
7. Morimoto M, Kanno H, Asai H, et al. Pyruvate kinase deficiency of mice associated with nonspherocytic hemolytic anemia and cure of the anemia by marrow transplantation without host irradiation. Blood. 1995;86:4323–4330.
8. Kanno H, Morimoto M, Fujii H, et al. Primary structure of murine red blood cell-type pyruvate kinase (PK) and molecular characterization of PK deficiency identified in the CBA strain. Blood. 1995;86: 3205–3210.
9. Aizawa S, Kohdera U, Hiramoto M, et al. Ineffective erythropoiesis in the spleen of a patient with pyruvate kinase deficiency. Am J Hematol. 2003;74:68–72.
10. Aizawa S, Harada T, Kanbe E, et al. Ineffective erythropoiesis in mutant mice with deficient pyruvate kinase activity. Exp Hematol. 2005; 33:1292–1298.
11. Kanno H, Fujii H, Hirono A, Miwa S. cDNA cloning of human R-type pyruvate kinase and identification of a single amino acid substitution (Thr384→Met) affecting enzymatic stability in a pyruvate kinase variant (PK Tokyo) associated with hereditary hemolytic anemia. Proc Natl Acad Sci U S A. 1991;88:8218–8221.
12. Beutler E, Blume KG, Kaplan JC, Loehr GW, Ramot B, Valentine WN. International Committee for Standardization in Haematology: recommended methods for red cell enzyme analysis. Br J Haematol. 1977;35:331–340.
13. Kanno J, Aisaki K, Igarashi K, et al. "Per cell" normalization method for mRNA measurement by quantitative PCR and microarrays. BMC Genomics. 2006;29:64.
14. Krones A, Jungermann K, Kietzmann T. Cross-talk between the signals hypoxia and glucose at the glucose response element of the L-type pyruvate kinase gene. Endocrinology. 2001;142:2707–2718.
15. Danial NN, Gramm CF, Scorrano L, et al. BAD and glucokinase reside in a mitochondrial complex that integrates glycolysis and apoptosis. Nature. 2003;424:952–956.
16. Shim H, Chun YS, Lewis BC, Dang CV. A unique glucose-dependent apoptotic pathway induced by c-Myc. Proc Natl Acad Sci U S A. 1998;95:1511–1516.
17. Brand K, Netzker R, Aulwurm U, et al. Control of thymocyte proliferation via redox-regulated expression of glycolytic genes. Redox Rep. 2000;5:52–54.
18. Shimizu T, Uehara T, Nomura Y. Possible involvement of pyruvate kinase in acquisition of tolerance to hypoxic stress in glial cells. J Neurochem. 2004;91:167–175.
19. Lee YJ, Kang IJ, Bunger R, Kang YH. Mechanisms of pyruvate inhibition of oxidant-induced apoptosis in human endothelial cells. Microvasc Res. 2003;66:91–101.
20. Basing E, Summer O, Schemer M, Bunger R. Antioxidant pyruvate inhibits cardiac formation of reactive oxygen species through changes in redox state. Am J Physiol Heart Circ Physiol. 2000;279:H2431–H2438.
21. Luzzatto L, Mehta A, Vulliamy T. Glucose 6-phosphate dehydrogenase. In: Scriver CR, Beaudet AL, Sly WS, Valle D, eds. The Metabolic & Molecular Bases of Inherited Disease. 8th ed.. New York: McGraw-Hill; 2001. p. 4517–4554.
22. Neumann CA, Krause DS, Carman CV, et al. Essential role for the peroxiredoxin Prdx1 in erythrocyte antioxidant defense and tumour suppression. Nature. 2003;424:561–565.
23. Lee TH, Kim SU, Yu SL, et al. Peroxiredoxin II is essential for sustaining life span of erythrocytes in mice. Blood. 2003;101:5033–5038.
24. Ferreira P, Morais L, Costa R, et al. Hydrops fetalis associated with erythrocyte pyruvate kinase deficiency. Eur J Pediatr. 2000;159: 481–482.
25. Bowman HS, McKusick VA, Dronamraju KR. Pyruvate kinase deficient hemolytic anemia in an Amish isolate. Am J Hum Genet. 1965;17:1–8.
26. Tanphaichitr VS, Suvatte V, Issaragrisil S, et al. Successful bone marrow transplantation in a child with red blood cell pyruvate kinase deficiency. Bone Marrow Transplant. 2000;26:689–690.

0090-9556/07/3510-1949–1955$20.00
DRUG METABOLISM AND DISPOSITION
Copyright © 2007 by The American Society for Pharmacology and Experimental Therapeutics
DMD 35:1949–1955, 2007

Vol. 35, No. 10
17327/3255799
Printed in U.S.A.

A Novel Mechanism for Polychlorinated Biphenyl-Induced Decrease in Serum Thyroxine Level in Rats

Yoshihisa Kato, Shin-ichi Ikushiro, Rie Takiguchi, Koichi Haraguchi, Nobuyuki Koga, Shinya Uchida, Toshiyuki Sakaki, Shizuo Yamada, Jun Kanno, and Masakuni Degawa

Kagawa School of Pharmaceutical Sciences, Tokushima Bunri University, Sanuki, Kagawa, Japan (Y.K.); Faculty of Engineering, Toyama Prefectural University, Toyama, Japan (S.I., T.S.); School of Pharmaceutical Sciences and Center of Excellence (COE) Program in the 21st Century, University of Shizuoka, Shizuoka, Japan (R.T., S.U., S.Y., M.D.); Daiichi College of Pharmaceutical Sciences, Fukuoka, Japan (K.H.); Faculty of Nutritional Sciences, Nakamura Gakuen University, Fukuoka, Japan (N.K.); and Division of Cellular & Molecular Toxicology, National Institute of Health Sciences, Tokyo, Japan (J.K.)

Received June 19, 2007; accepted July 12, 2007

ABSTRACT:

We have previously suggested that the decrease in the levels of serum total thyroxine (T_4) and free T_4 by a single administration to rats of Kanechlor-500 (KC500) at a dose of 100 mg/kg is not necessarily dependent on the increase in hepatic T_4-UDP-glucuronosyltransferase (UDP-GT). In the present study, we determined whether or not a consecutive treatment with KC500 at a relatively low dose (10 mg/kg i.p., once daily for 10 days) results in a decrease in the level of serum total T_4 and further investigated an exact mechanism for the KC500-induced decrease in the T_4. At 4 days after final treatment with KC500, the serum total T_4 and free T_4 levels were markedly decreased in both Wistar and UGT1A-deficient Wistar (Gunn) rats, whereas significant increases in hepatic T_4-UDP-GT activity were observed in Wistar rats but not in Gunn rats. The level of serum thyroid-stimulating hormone was not significantly changed in either Wistar or Gunn rats. Clearance from serum of the [^{125}I]T_4 administered to the KC500-pretreated Wistar and Gunn rats was faster than that to the corresponding control (KC500-untreated) rats. The accumulated level of [^{125}I]T_4 was increased in several tissues, especially the liver, in the KC500-pretreated rats. The present findings demonstrated that a consecutive treatment with KC500 resulted in a significant decrease in the level of serum total T_4 in both Wistar and Gunn rats and further indicated that the KC500-induced decrease would occur through increase in accumulation of T_4 in several tissues, especially the liver, rather than increase in hepatic T_4-UDP-GT activity.

Most polychlorinated biphenyls (PCBs) are known to decrease the level of serum thyroid hormone and to increase the activity of hepatic drug-metabolizing enzymes in rats (Van Birgelen et al., 1995; Craft et al., 2002). As possible mechanisms for the PCB-induced decrease in the level of serum thyroid hormone, enhancement of thyroid hormone metabolism by PCB and displacement of the hormone from serum transport proteins, including transthyretin (TTR), by PCB and its ring-hydroxylated metabolites are considered (Barter and Klaassen, 1992a, 1994; Brouwer et al., 1998). In particular, the decrease in the level of serum thyroxine (T_4) by 3,3′,4,4′,5-pentachlorobiphenyl, Aroclor 1254, and 2,3,7,8-tetrachlorodibenzo-*p*-dioxin in rats is believed to occur mainly through induction of the UDP-glucuronosyltransferases (UDP-GTs), especially UGT1A subfamily enzymes, responsible for glucuronidation of T_4 (Barter and Klaassen, 1994; Van Birgelen et al., 1995). However, the magnitude of decrease in the level of serum total T_4 is not necessarily correlated with that of increase in T_4-UDP-GT activity (Craft et al., 2002; Hood et al., 2003). Furthermore, we have reported that in Kanechlor-500 (KC500)-treated mice, serum T_4 level decreased without an increase in T_4-UDP-GT activity (Kato et al., 2003) and that the decrease in serum total T_4 level by a single administration of either KC500 or 2,2′,4,5,5′-pentachlorobiphenyl occurred even in UGT1A-deficient Wistar (Gunn) rats (Kato et al., 2004). Thus, an exact mechanism for the PCB-induced decrease in the level of serum thyroid hormone remains unclear. To date, most studies on biological effects of PCB have been performed using experimental animals treated once at a high dose (more than 100 mg/kg body weight), and the effect of the consecutive treatment at a low dose has been little reported. Humans and wild animals are exposed to a wide variety of environmental chemicals, including PCB, at a low level over a long period of time. Therefore, a study on biological effects by consecutive treatment with PCB at a low dose would be very important.

In the present study, therefore, we examined whether or not a consecutive treatment with KC500 at a relatively low dose (10 mg/kg i.p., once daily for 10 days) results in decrease in the level of serum total T_4 and further discussed a mechanism underlying the PCB-induced decrease in the T_4.

This work was supported in part by the Grant-in-Aid for Scientific Research (C) (no. 18510061; Y.K.) and for Scientific Research (B) (no. 19310042; K.H., Y.K.) from Japan Society for the Promotion of Science, and by a Health and Labour Sciences Research Grant for Research on Risk of Chemical Substances (H16-Kagaku-003; Y.K.) from the Ministry of Health, Labour and Welfare of Japan.

Article, publication date, and citation information can be found at http://dmd.aspetjournals.org.

doi:10.1124/dmd.107.017327.

ABBREVIATIONS: PCB, polychlorinated biphenyl; KC500, Kanechlor-500; T_3, triiodothyronine; T_4, thyroxine; TTR, transthyretin; TSH, thyroid-stimulating hormone; UDP-GT, UDP-glucuronosyltransferase.

Materials and Methods

Chemicals. Panacete 810 (medium-chain triglycerides) was purchased from Nippon Oils and Fats Co. Ltd. (Tokyo, Japan). The [^{125}I]T_4, radiolabeled at the 5′-position of the outer ring, was obtained from PerkinElmer Life and Analytical Sciences (Waltham, MA). The KC500 used in the present experiments contains 2,2′,5,5′-tetrachlorobiphenyl (5.6% of total PCBs), 2,2′,3,5′,6-pentachlorobiphenyl (6.5%), 2,2′,4,5,5′-pentachlorobiphenyl (10%), 2,3,3′,4′,6-pentachlorobiphenyl (7.4%), 2,3′,4,4′,5-pentachlorobiphenyl (7.7%), 2,2′,3,4,4′,5′-hexachlorobiphenyl (5.6%), and 2,2′,4,4′,5,5′-hexachlorobiphenyl (5.4%) as major PCB congeners (Haraguchi et al., 2005). All the other chemicals used herein were obtained commercially in appropriate grades of purity.

Animal Treatments. Male Wistar rats (160–200 g) and UGT1A-deficient Wistar rats (Gunn rats, 190–260 g) were obtained from Japan SLC., Inc. (Shizuoka, Japan). Male Wistar and Gunn rats were housed three or four per cage with free access to commercial chow and tap water, maintained on a 12-h dark/light cycle (8:00 AM to 8:00 PM light) in an air-controlled room (temperature, 24.5 ± 1°C; humidity, 55 ± 5%), and handled with human care under the guidelines of the University of Shizuoka (Shizuoka, Japan). Rats received consecutive intraperitoneal injections of KC500 (10 mg/kg) dissolved in Panacete 810 (5 ml/kg) at 24-h intervals for 10 days. Control animals were treated with vehicle alone (5 mg/kg).

In Vivo Study. Rats were killed by decapitation 4 days after the final administration of KC500. The liver was removed, and hepatic microsomes were prepared according to the method of Kato et al. (1995) and stored at −85°C until use. Blood was collected from each animal between 10:30 and 11:30 AM. After clotting at room temperature, serum was separated by centrifugation and stored at −50°C until use.

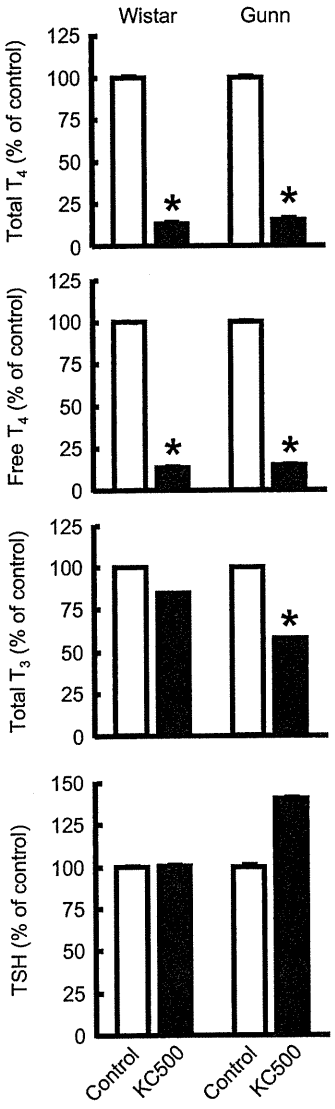

FIG. 1. Effects of KC500 on levels of serum total T_4, free T_4, total T_3, and TSH in Wistar and Gunn rats. Animals were killed 4 days after the final administration of KC500 (10 mg/kg i.p., once daily for 10 days), and levels of serum thyroid hormones were measured as described under *Materials and Methods*. Constitutive levels: total T_4, 4.29 ± 0.38 (Wistar, n = 5) and 5.80 ± 0.32 μg/dl (Gunn, n = 5); free T_4, 2.17 ± 0.16 (Wistar, n = 5) and 2.71 ± 0.17 ng/dl (Gunn, n = 5); total T_3, 0.34 ± 0.03 (Wistar, n = 6) and 0.96 ± 0.05 ng/ml (Gunn, n = 4); TSH, 4.89 ± 0.33 (Wistar, n = 5) and 7.48 ± 1.14 ng/ml (Gunn, n = 5). Each column represents the mean ± S.E. (vertical bars) for five to six animals. *, $P < 0.01$, significantly different from each control.

TABLE 1

Effects of KC500 on the activity of hepatic microsomal alkoxyresorufin O-dealkylases in Wistar and Gunn rats

Animals were killed at 4 days after the final administration of KC500 (10 mg/kg i.p., once daily for 10 days). The values shown are expressed as the mean ± S.E. for four to five animals.

Substrates	Wistar		Gunn	
	Control	KC500	Control	KC500
	nmol/mg protein/min		*nmol/mg protein/min*	
7-Benzyloxyresorufin	0.07 ± 0.01	3.34 ± 0.33*	0.03 ± 0.003	1.08 ± 0.27*
7-Pentoxyresorufin	0.03 ± 0.003	0.43 ± 0.05*	0.02 ± 0.003	0.22 ± 0.05*
7-Ethoxyresorufin	0.14 ± 0.01	9.02 ± 0.09*	0.21 ± 0.01	2.21 ± 0.29*

* $P < 0.05$, significantly different from each control.

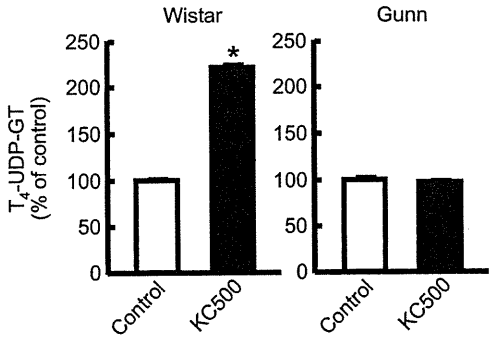

FIG. 2. Effects of KC500 on the activity of hepatic microsomal UDP-glucuronyltransferase in Wistar and Gunn rats. Each column represents the mean ± S.E. (vertical bars) for five to six animals. Constitutive levels: T_4-UDP-GT, 14.17 ± 1.11 pmol/mg protein/min (Wistar) and 6.36 ± 1.34 pmol/mg protein/min (Gunn). *, $P < 0.01$, significantly different from each control.

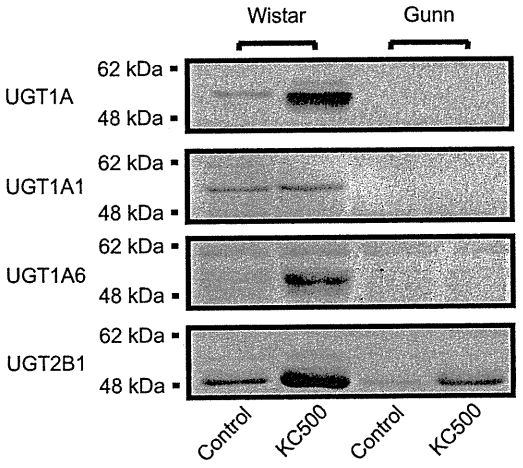

FIG. 3. Representative Western blot profiles for hepatic microsomal UGT isoforms in the KC500-treated Wistar and Gunn rats.

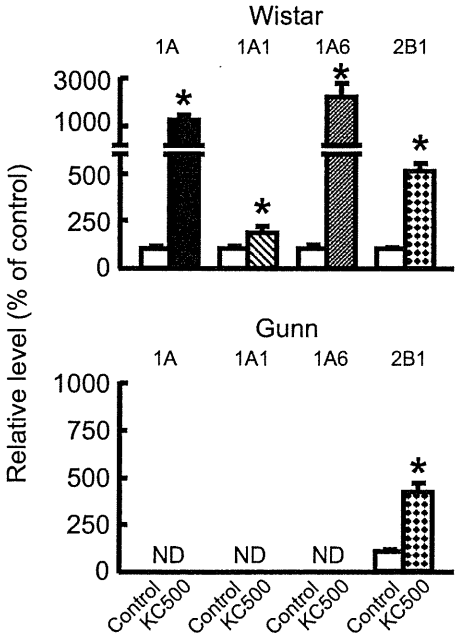

FIG. 4. Effects of KC500 on levels of hepatic microsomal UGT isoforms in Wistar and Gunn rats. The isolated bands responsible for UGT isoforms, which are shown in Fig. 3, were densitometrically quantified as described under *Materials and Methods*. The data are represented as the mean ± S.E. (vertical bars) for five to six animals. *, $P < 0.05$, significantly different from each control. ND, not detectable.

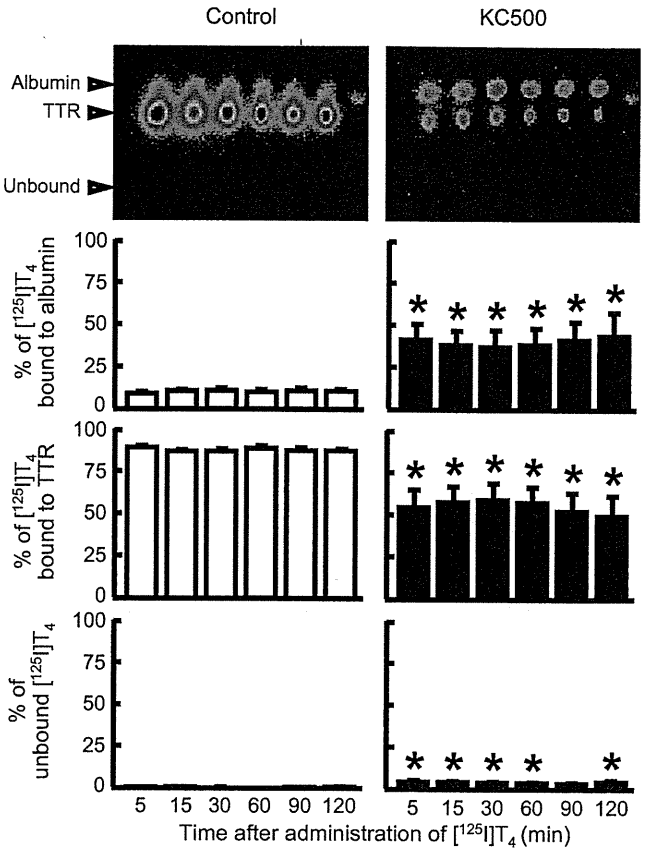

FIG. 5. Effects of KC500 on the binding of $[^{125}I]T_4$ to serum proteins in Wistar rats. Amounts of $[^{125}I]T_4$ bound to the serum proteins were assessed by the method described under *Materials and Methods*. Each column represents the mean ± S.E. (vertical bars) for three to six animals. *, $P < 0.05$, significantly different from each control.

Analysis of serum hormones. Levels of total T_4, free T_4, total triiodothyronine (T_3), and thyroid-stimulating hormone (TSH) were measured by radioimmunoassay using Total T4 and Free T4 kits (Diagnostic Products Corporation, Los Angels, CA), the Triiodothyronine kit GammaCoat T_3 II (DiaSorin Inc., Stillwater, MN), and the rTSH $[^{125}I]$ Biotrak assay system (GE Healthcare UK, Ltd., Little Chalfont, Buckinghamshire, UK), respectively.

Hepatic microsomal enzyme assays. Hepatic microsomal fraction was prepared according to the method described previously (Kato et al., 1995), and the amount of hepatic microsomal protein was determined by the method of Lowry et al. (1951) with bovine serum albumin as a standard. Microsomal *O*-dealkylase activities of 7-benzyloxy-, 7-ethoxy-, and 7-pentoxyresorufins were determined by the method of Burke et al. (1985).

Hepatic T_4-metabolizing enzyme assay. The activity of microsomal UDP-GT toward T_4 (T_4-UGT activity) was determined by the methods of Barter and Klaassen (1992b).

Western blot analysis. The polyclonal anti-peptide antibodies against the common region of UGT1A isoforms and specific antibodies against UGT1A1, UGT1A6, and UGT2B1, which were established by Ikushiro et al. (1995, 1997), were used. Western blot analyses for microsomal UGT isoforms were performed by the method of Luquita et al. (2001). The bands corresponding to UGT1A1, UGT1A6, and UGT2B1 on a sheet were detected using chemical luminescence (ECL detection kit; GE Healthcare UK, Ltd.), and the level of each protein was determined densitometrically with LAS-1000 (Fuji Photo Film. Co., Ltd., Tokyo, Japan).

Ex Vivo Study. At 4 days after a consecutive 10-day treatment with KC500, the rats were anesthetized with a saline (2 ml/kg) containing sodium pentobarbital (25 mg/ml) and potassium iodide (1 mg/ml). The femoral artery was cannulated (polyethylene tube SP31; Natsume Inc., Tokyo, Japan) and primed with heparinized saline (33 units/ml), and then the animal's body was warmed to 37°C. Fifteen minutes later, the rats were given i.v. 1 ml of $[^{125}I]T_4$ (15 μCi /ml) dissolved in the saline containing 10 mM NaOH and 1% normal rat serum.

Clearance of $[^{125}I]T_4$ from serum. The study on the clearance of $[^{125}I]T_4$ from serum was performed according to the method of Oppenheimer et al. (1968). In brief, after the administration of $[^{125}I]T_4$, a portion (0.3 ml) of blood was sampled from the artery at the indicated times, and serum was prepared and stored at −50°C until use. Two aliquots (15 μl each) were taken from each serum sample for determining $[^{125}I]T_4$ level by a gamma counter (COBRA II AUTO-GAMMA 5002; PerkinElmer Life and Analytical Sciences).

Analysis of $[^{125}I]T_4$ bound to serum proteins. The levels of serum $[^{125}I]T_4$-albumin and $[^{125}I]T_4$-TTR complexes were determined according to the method of Davis et al. (1970). In brief, serum was diluted in 100 mM phosphate buffer (pH 7.4) containing 1 mM EDTA, 1 mM dithiothreitol, and 30% glycerol, and subjected to electrophoresis on 4 to 20% gradient native polyacrylamide gels PAG Mid "Daiichi" 4/20 (Daiichi Pure Chemicals Co., Ltd., Tokyo, Japan). The electrophoresis was performed at 4°C for 11 h at 20 mA in the 0.025 M Tris buffer (pH 8.4) containing 0.192 M glycine. The human albumin and TTR, which were incubated with $[^{125}I]T_4$, were also applied on the gel as templates. After the electrophoresis, a gel was dried and radioautographed for 20 h at room temperature using Imaging Plate 2040 (Fuji Photo Film Co., Ltd.). The levels of $[^{125}I]T_4$-albumin and $[^{125}I]T_4$-TTR in serum were determined by counting the gel fractions identified from Bio Imaging Analyzer (BAS-2000II IP Reader; Fuji Photo Film Co., Ltd.).

Tissue distribution of $[^{125}I]T_4$. The study on the tissue distribution of $[^{125}I]T_4$ was performed according to the modified method of Oppenheimer et al. (1968). In brief, at 60 min after administration of $[^{125}I]T_4$ to KC500-pretreated rats, blood was sampled from abdominal aorta. Then, cerebrum, cerebellum, pituitary gland, thyroid gland, sublingual gland, submandibular gland, thymus, heart, lung, liver, kidney, adrenal gland, spleen, pancreas, testis, prostate gland, seminal vesicle, stomach, duodenum, jejunum, ileum, cecum, brown fat, skeletal muscle, bone marrow skin, spinal cord, and fat were removed and weighed. Radioactivities in serum and the tissues were determined by a gamma-counter (COBRA II AUTO-GAMMA5002; PerkinElmer Life and Analytical Sciences), and amounts of $[^{125}I]T_4$ in various tissues were shown as ratios of tissue to serum.

Statistics. The data obtained were statistically analyzed according to Stu-

dent's *t* test or Dunnett's test after analysis of variance. In addition, data of the clearance of [^{125}I]T_4 from serum and analysis of [^{125}I]T_4 bound to serum proteins were statistically analyzed according to the Newman-Keuls test after analysis of variance. The pharmacokinetic parameters of [^{125}I]T_4 were estimated with noncompartmental methods as described previously (Tabata et al., 1999).

Results

Serum Hormone Levels. Effects of KC500 on levels of serum thyroid hormones were examined in Wistar and Gunn rats (Fig. 1). In both Wistar and Gunn rats, KC500 treatment resulted in decreases of the serum total T_4 and free T_4, and the magnitude of the decrease in each serum thyroid hormone was almost the same in both strains of rats. On the other hand, a significant decrease in the level of serum total T_3 was observed in Gunn rats but not in Wistar rats. In addition, no significant change in TSH level was observed in either Wistar or Gunn rats.

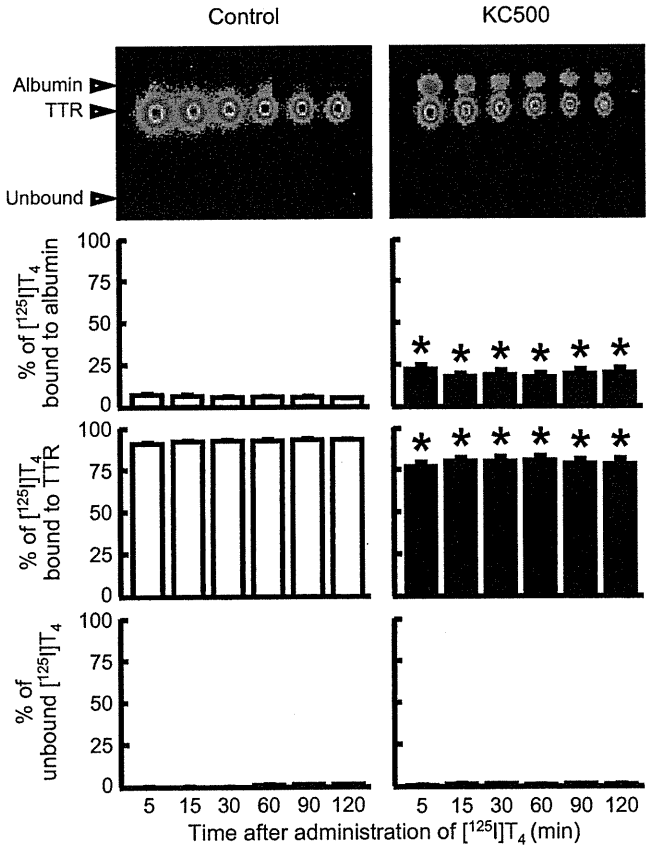

FIG. 6. Effects of KC500 on the binding of [^{125}I]T_4 to serum proteins in Gunn rats. Amounts of [^{125}I]T_4 bound to the serum proteins were assessed by the method described under *Materials and Methods*. Each column represents the mean ± S.E. (vertical bars) for four to five animals. *, $P < 0.05$, significantly different from each control.

Hepatic Drug-Metabolizing Enzymes. Effects of KC500 on hepatic microsomal activities of benzyloxyresorufin *O*-dealkylase (CYP2B1/2 and CYP3A1/2), pentoxyresorufin *O*-dealkylase (CYP2B1/2), and ethoxyresorufin *O*-dealkylase (CYP1A1/2) were examined in Wistar and Gunn rats. In both Wistar and Gunn rats, these enzyme activities were significantly increased by KC500 (Table 1), and the increase in each enzyme activity was much greater in Wistar rats than in Gunn rats.

Hepatic T_4-Metabolizing Enzyme Activities. T_4 glucuronidation is primarily mediated by hepatic T_4-UDP-GTs, such as UGT1A1 and UGT1A6, in the rat liver (Visser, 1996), and a chemical-mediated induction of the enzymes is considered to contribute to the decrease in the level of serum total T_4. Therefore, we examined effects of KC500 on hepatic microsomal T_4-UDP-GT activity in Wistar and Gunn rats. Constitutive activity of T_4-UDP-GT was approximately 2.2-fold higher in Wistar rats than in Gunn rats. Treatment with KC500 resulted in significant increase of T_4-UDP-GT activity in Wistar rats but not in Gunn rats (Fig. 2).

Western Blot Analysis for UGT1As. Levels of the proteins responsible for UGT1A enzymes, UGT1A1 and UGT1A6, were increased by KC500 treatment in Wistar rats but not in Gunn rats (Figs. 3 and 4). In addition, no expression of the UGT1A enzymes was confirmed in Gunn rats. On the other hand, the level of UGT2B1 was significantly increased by KC500 in both Wistar and Gunn rats, and magnitudes of the increase in both strains of rats were almost the same (Figs. 3 and 4).

Serum Proteins Bound to [^{125}I]T_4. The effects of KC500 on the binding of [^{125}I]T_4 to serum proteins, TTR, and albumin were examined in Wistar and Gunn rats (Figs. 5 and 6). In both Wistar and Gunn rats, pretreatment with KC500 resulted in a significant decrease in the level of [^{125}I]T_4-TTR complex, whereas it resulted in a significant increase in the level of [^{125}I]T_4 bound to albumin (Figs. 5 and 6).

Clearance of [^{125}I]T_4 from Serum. After an i.v. administration of [^{125}I]T_4 to the KC500-pretreated Wistar and Gunn rats, concentrations of [^{125}I]T_4 in sera were measured at the indicated times (Fig. 7). In both Wistar and Gunn rats, pretreatment with KC500 promoted the clearance of [^{125}I]T_4 from serum, and their serum [^{125}I]T_4 levels were decreased to approximately 40% of the initial level within 5 min. In the KC500-untreated Wistar and Gunn rats, serum [^{125}I]T_4 levels were gradually decreased to approximately 40% of the initial level at 120 min later. The serum pharmacokinetic parameters of the [^{125}I]T_4 estimated from these data (Fig. 7) were summarized in Table 2. The mean total body clearances (CL_{tb}) of [^{125}I]T_4 in the KC500-pretreated rats were 2.4 and 2.9 times, respectively, greater than those in the corresponding control rats. The steady-state volumes of distribution (Vd_{ss}) in the KC500-pretreated rats were 1.6 and 2.4 times, respectively, larger than those in the corresponding control rats.

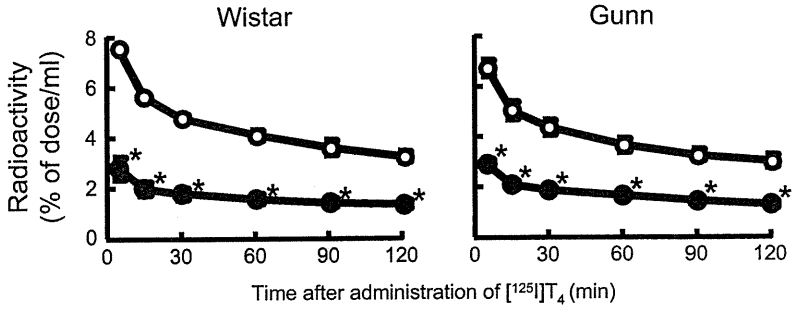

FIG. 7. Effects of KC500 on the clearance of [^{125}I]T_4 from serum in Wistar and Gunn rats. The amount of serum [^{125}I]T_4 was measured at the indicated times after the i.v. administration of [^{125}I]T_4. Each point represents the mean ± S.E. (vertical bars) for four to eight animals. *, $P < 0.001$, significantly different from each control. ○, control; ●, KC500.

Tissue Distribution of [^{125}I]T_4. The tissue-to-serum concentration ratio (K_p value) and distribution level of [^{125}I]T_4 in tissue after the administration of [^{125}I]T_4 to the KC500-pretreated Wistar and Gunn rats are shown in Figs. 8 and 9, respectively. K_p values of the thyroid gland and liver were the greatest among those of the tissues examined in either Wistar or Gunn rats (Fig. 8). In addition, K_p values in all the tissues examined, with the exception of the testis and ileum, were greater in KC500-pretreated Wistar rats than those in the corresponding control (KC500-untreated) rats. K_p values in the thyroid gland, liver, and jejunum in the KC500-pretreated Wistar and Gunn rats were 1.6 to 1.8, 3.3 to 3.8, and 4.7 to 11.5 times, respectively, higher than those in corresponding control rats (Fig. 8).

In the control Wistar and Gunn rats, the accumulation level of [^{125}I]T_4 was highest in the liver, among the tissues examined (Fig. 9). In both Wistar and Gunn rats, pretreatment with KC500 resulted in an increase in the accumulation level in the liver, and the levels increased to more than 40% of the [^{125}I]T_4 dosed (Fig. 9). Likewise, significant increase in accumulation of [^{125}I]T_4 was observed in the jejunum (Fig. 9). In addition, significant increases in the liver weight and accumulation level (per g liver) of [^{125}I]T_4 occurred in KC500-pretreated Wistar rats, but not in Gunn rats (Tables 3 and 4).

Discussion

In the present study, we found that consecutive treatment with KC500 (10 mg/kg i.p., once daily for 10 days; total dose, 100 mg/kg) promoted accumulation of T_4 in several tissues, especially the liver, and resulted in a drastic decrease in the levels of serum total T_4 and free T_4 in both Wistar and Gunn (UGT1A-deficient) rats. Thus, a decrease in the level of serum total T_4 is also observed in the Wistar and Gunn rats treated with KC500 (a single i.p. administration at a dose of 100 mg/kg) (Kato et al., 2004). In addition, constitutive levels of serum total T_4 and T_3 were higher in Gunn rats than in Wistar rats, and the results were identified with those as previously described by Benathan et al. (1983). The difference in constitutive level of serum thyroid hormone between Wistar and Gunn rats seems to be dependent on differences in the level and/or activity of T_4/T_3-UDP-GTs.

As a possible explanation for a chemical-induced decrease in serum thyroid hormones, a hepatic T_4-UDP-GT-dependent mechanism is generally considered, because T_4-UDP-GT inducers, including PCB, phenobarbital, 3-methylcholanthrene, pregnenolone-16α-carbonitrile, and clobazam, show strong activities for decreasing the level of serum total thyroid hormones, including T_4 and T_3 (Barter and Klaassen, 1994; Van Birgelen et al., 1995; Miyawaki et al., 2003). However, among the experimental animals treated with a T_4-UDP-GT inducer, the difference in magnitude of decrease in the level of serum total T_4 is not necessarily correlated with that of hepatic T_4-UDP-GT activity (Craft et al., 2002; Hood et al., 2003; Kato et al., 2003). Our present and previous results (Kato et al., 2004, 2005) using Wistar and Gunn rats support a hypothesis that significant decrease in the level of serum total thyroid hormones by either PCB or phenobarbital occurs primarily in a hepatic T_4-UDP-GT-independent pathway.

As a possible mechanism for the PCB-induced decrease in serum T_4 level, an increase in hepatic drug-metabolizing enzymes might be considered. However, these are induced to a greater extent in the Wistar rats than in the Gunn rats, whereas magnitudes of decrease in serum T_4 level in Wistar and Gunn rats were almost the same. Accordingly, the KC500-induced decrease in serum T_4 level is thought to be independent of the KC500-induced drug-metabolizing enzymes, including UDT-GTs and cytochromes P450.

As the factors regulating the level of serum total T_4, serum TSH, hepatic type I iodothyronine deiodinase, and TTR are known. However, no significant change in the level of serum TSH occurs in the PCB-treated rats (Liu et al., 1995; Hood et al., 1999; Hallgren et al., 2001; Kato et al., 2004). Hepatic type I iodothyronine deiodinase activity was significantly decreased in Wistar and Gunn rats by KC500 (Kato et al., 2004). On the other hand, a TTR-associated pathway might be considered as an explanation for the PCB-induced decrease in the level of serum total

TABLE 2

Pharmacokinetic parameters for [^{125}I]T_4 after the administration of [^{125}I]T_4 to the KC500-pretreated Wistar and Gunn rats

The experimental conditions were the same as those described in Fig. 7. The values shown are expressed as the mean ± S.E. for four to seven animals.

Animal	Treatment	Mean Total Body Clearance × 100	Distribution Volume
		ml/min	*ml*
Wistar	Control	7.82 ± 0.59	17.91 ± 0.52
	KC500	18.85 ± 3.49*	51.51 ± 6.34*
Gunn	Control	8.44 ± 0.22	20.21 ± 1.79
	KC500	13.84 ± 0.88*	48.91 ± 3.50*

* $P < 0.05$, significantly different from each control.

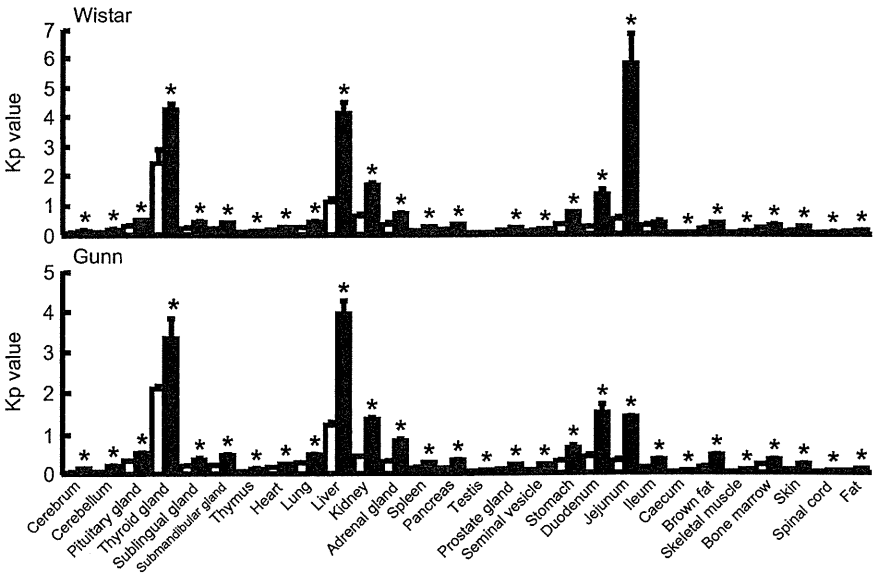

FIG. 8. Tissue-to-serum concentration ratio (K_p value) of [^{125}I]T_4 in various tissues after administration of [^{125}I]T_4 to the KC500-pretreated Wistar and Gunn rats. KC500 (10 mg/kg) was given i.p. to animals once daily for 10 days, and then, the animals were administered i.v. [^{125}I]T_4. At 60 min after administration of [^{125}I]T_4, the radioactivity in each tissue was measured. Each column represents the mean ± S.E. (vertical bars) for three to six animals. *, $P < 0.05$, significantly different from each control. □, control; ■, KC500.

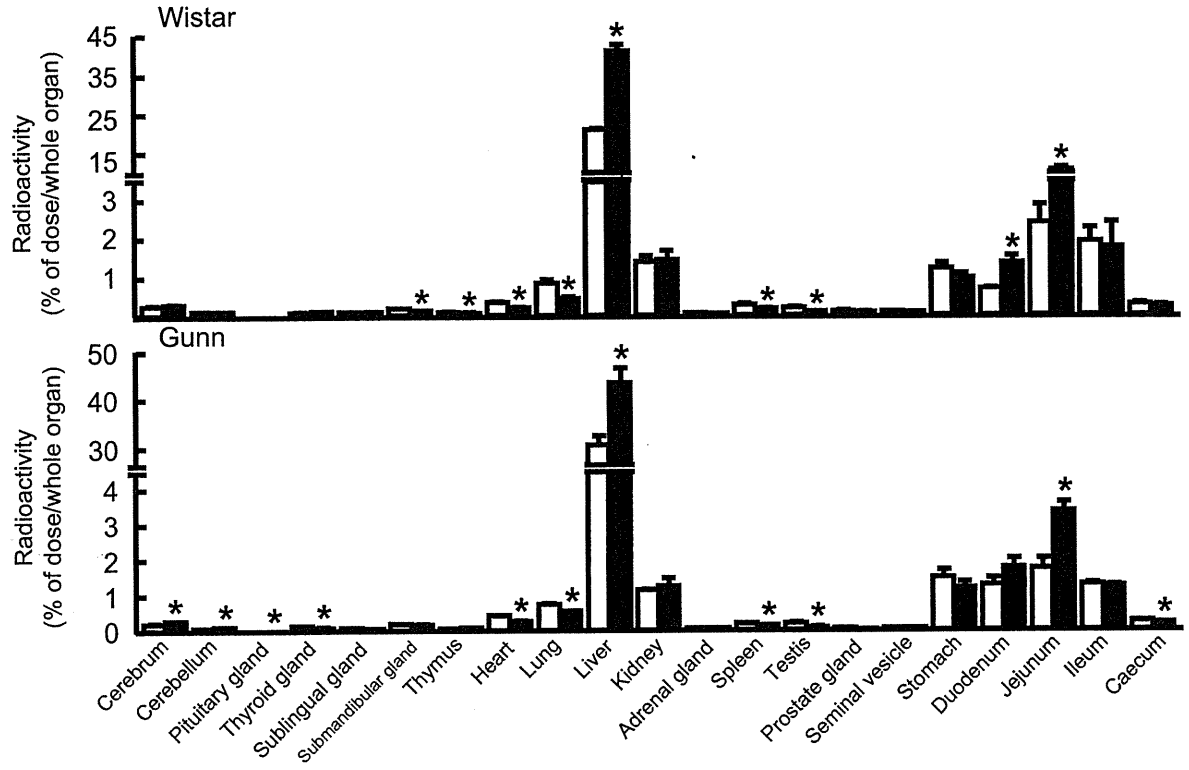

FIG. 9. Tissue distribution of [^{125}I]T_4 after administration of [^{125}I]T_4 to the KC500-pretreated Wistar and Gunn rats. The experimental conditions were the same as those described in Fig. 8. Each column represents the mean ± S.E. (vertical bars) for four to six animals. *, $P < 0.05$, significantly different from each control. □, control; ■, KC500.

TABLE 3

Liver weights after the administration of KC500 to Wistar and Gunn rats

Animals were killed at 4 days after the final administration of KC500 (10 mg/kg i.p., once daily for 10 days). The values shown are expressed as the mean ± S.E. for four to six animals.

Animal	Liver Weight	
	Control	KC500
	% of body weight	
Wistar	3.07 ± 0.04	3.81 ± 0.17*
Gunn	3.25 ± 0.08	3.38 ± 0.10

*$P < 0.01$, significantly different from each control.

TABLE 4

Accumulation of [^{125}I]T_4 in the KC500-pretreated Wistar and Gunn rat livers

The experimental conditions were the same as those described in Fig. 8. The values shown are expressed as the mean ± S.E. for four to six animals.

Animal	[^{125}I]T_4	
	Control	KC500
	% of dose/g liver	
Wistar	3.86 ± 0.18	6.01 ± 0.24*
Gunn	4.74 ± 0.43	6.33 ± 0.62

* $P < 0.001$, significantly different from each control.

T_4, because PCB and its ring-hydroxylated metabolites act as T_4 antagonists to TTR (Lans et al., 1993; Brouwer et al., 1998; Meerts et al., 2002; Kato et al., 2004). Thus, competitive inhibition by PCB and/or its metabolites would promote a decrease in the level of serum total T_4. In the present study, significant decrease in the level of [^{125}I]T_4 bound to serum TTR and increase in the level of [^{125}I]T_4 bound to serum albumin occurred in both KC500-pretreated Wistar and Gunn rats, suggesting that PCB and/or its metabolite(s) inhibit the formation of serum T_4-TTR complex.

Thus, inhibition of the T_4-TTR formation might lead to change in the tissue distribution of T_4. Therefore, to clarify this, we administered [^{125}I]T_4 to KC500-pretreated Wistar and Gunn rats and, thereafter, determined the levels of [^{125}I]T_4 in their tissues. In addition, since [^{125}I]T_4 in either plasma or tissues is known to be stable during 48 h (Oppenheimer et al., 1968), the radioactivity detected in the serum and tissues would be attributed to [^{125}I]T_4 in each tissue. Marked increases in the mean total body clearance of [^{125}I]T_4 and in the steady-state distribution volume of [^{125}I]T_4 were observed in the KC500-pretreated rats. A tissue-to-serum concentration ratio (K_p value) was greater in several tissues, especially the liver, of the KC500-pretreated Wistar and Gunn rats than in the corresponding control (KC500-untreated) rat tissues. In addition, in both KC500-pretreated Wistar and Gunn rats, more than 40% of the [^{125}I]T_4 dosed was accumulated in the liver.

In conclusion, the present findings confirmed that PCB-induced decrease in serum T_4 occurs not only in Wistar rats but also in Gunn (UGT1A-deficient) rats and further led to a hypothesis that the PCB-induced decrease occurs through increase in accumulation (transportation from serum to liver) of T_4 in the liver, rather than through induction of hepatic T_4-UDP-GT. In addition, the increased accumulation in the liver might be attributed to the PCB- and its metabolite(s)-mediated inhibition of formation of serum T_4-TTR complex.

References

Barter RA and Klaassen CD (1992a) UDP-glucuronosyltransferase inducers reduce thyroid hormone levels in rats by an extrathyroidal mechanism. *Toxicol Appl Pharmacol* **113**:36–42.
Barter RA and Klaassen CD (1992b) Rat liver microsomal UDP-glucuronosyltransferase activity